Journal of Structural Geology, Vol. 12, No. 2, pp. 185–206, 1990
Printed in Great Britain

0191-8141/90 $03.00+0.00
Pergamon Press plc

Flexure and faulting of sedimentary host rocks during growth of igneous domes, Henry Mountains, Utah

MARIE D. JACKSON

U.S. Geological Survey, Hawaii National Park, HI 96718, U.S.A.

and

DAVID D. POLLARD

Departments of Applied Earth Sciences & Geology, Stanford University, Stanford, CA 94305, U.S.A.

(*Received* 23 *November* 1988; *accepted in revised form* 22 *June* 1989)

Abstract—A sequence of sedimentary rocks about 4 km thick was bent, stretched and uplifted during the growth of three igneous domes in the southern Henry Mountains. Mount Holmes, Mount Ellsworth and Mount Hillers are all about 12 km in diameter, but the amplitudes of their domes are about 1.2, 1.85 and 3.0 km, respectively. These mountains record successive stages in the inflation of near-surface diorite intrusions that are probably laccolithic in origin. The host rocks deformed along networks of outcrop-scale faults, or deformation bands, marked by crushed grains, consolidation of the porous sandstone and small displacements of sedimentary beds. Zones of deformation bands oriented parallel to the beds and formation contacts subdivided the overburden into thin mechanical layers that slipped over one another during doming.

Measurements of outcrop-scale fault populations at the three mountains reveal a network of faults that strikes at high angles to sedimentary beds which themselves strike tangentially about the domes. These faults have normal and reverse components of slip that accommodated bending and stretching strains within the strata. An early stage of this deformation is displayed at Mount Holmes, where states of stress computed from three fault samples correlate with the theoretical distribution of stresses resulting from bending of thin, circular, elastic plates. Field observations and analysis of frictional driving stresses acting on horizontal planes above an opening-mode dislocation, as well as the paleostress analysis of faulting, indicate that bedding-plane slip and layer flexure were important components of the early deformation. As the amplitude of doming increased, radial and circumferential stretching of the strata and rotation of the older faults in the steepening limbs of the domes increased the complexity of the fault patterns. Steeply-dipping, map-scale faults with dip-slip displacements indicate a late-stage jostling of major blocks over the central magma chamber. Radial dikes pierced the dome and accommodated some of the circumferential stretching.

INTRODUCTION

THE Henry Mountains (Fig. 1) are one of several laccolithic mountain ranges located near the center of the Colorado Plateau. There, in 1877, G. K. Gilbert observed that layers of sedimentary rock form domes, upturned at the periphery, and flattened over the top of porphyritic diorite intrusions. Recognizing the concordant nature of the intrusions underlying the domes, Gilbert hypothesized that they grew from sills and expanded into laccoliths by bending, stretching, and lifting the overlying beds.

Geological and geophysical data (Jackson & Pollard 1988) suggest that the intrusions underlying the three large southern Henry Mountains domes originated as sills and thickened by faulting and flexing the overburden, in part as Gilbert (1877) envisioned. K–Ar dating of Henry Mountains diorite porphyry by Armstrong (1969) gives Eocene ages, 44–48 Ma. Sullivan (1987), however, has found younger ages for these rocks, 20–29 Ma, using fission-track methods. Mount Holmes, Mount Ellsworth and Mount Hillers uplifted about 4 km of Permian through Tertiary overburden about 1.2, 1.8 and 3.0 km, respectively. These sedimentary beds strike tangentially about the domes and show a strong axial symmetry around all three mountains. In radial cross-sections, the flexed strata have a doubly-hinged shape: a central limb of nearly constant dip joins a concave-downwards upper hinge and a concave-upwards lower hinge. The central limb dips 20° at Mount Holmes, 50–55° at Mount Ellsworth and 75–85° at Mount Hillers. Cross-sections (Figs. 2–4) show that the radii of the domes are within the range of 5–7 km but that the curvature of the beds is concentrated within radii of less than 4 km. The distal portion of each flexure is composed of a gently-dipping peripheral limb 3–4 km long, presumably underlain by minor sills and laccoliths.

Jackson & Pollard's (1988) results are not in agreement with C. B. Hunt's (1953, pp. 121–124, 148–149) hypothesis that the large central intrusions underlying the Henry Mountains domes are tall, pipe-like, discordant stocks, which both domed the sedimentary host rocks and pushed them aside to create room for the magma. For example, cross-sections of the strata forming the domes (Figs. 2–4) are inconsistent with buckling of strata that are loaded by a radially expanding stock (see Jackson & Pollard 1988, fig. 18).

Recently, new experimental and analytical work has investigated the mechanisms of host rock deformation over laccolithic intrusions. Withjack & Scheiner (1982)

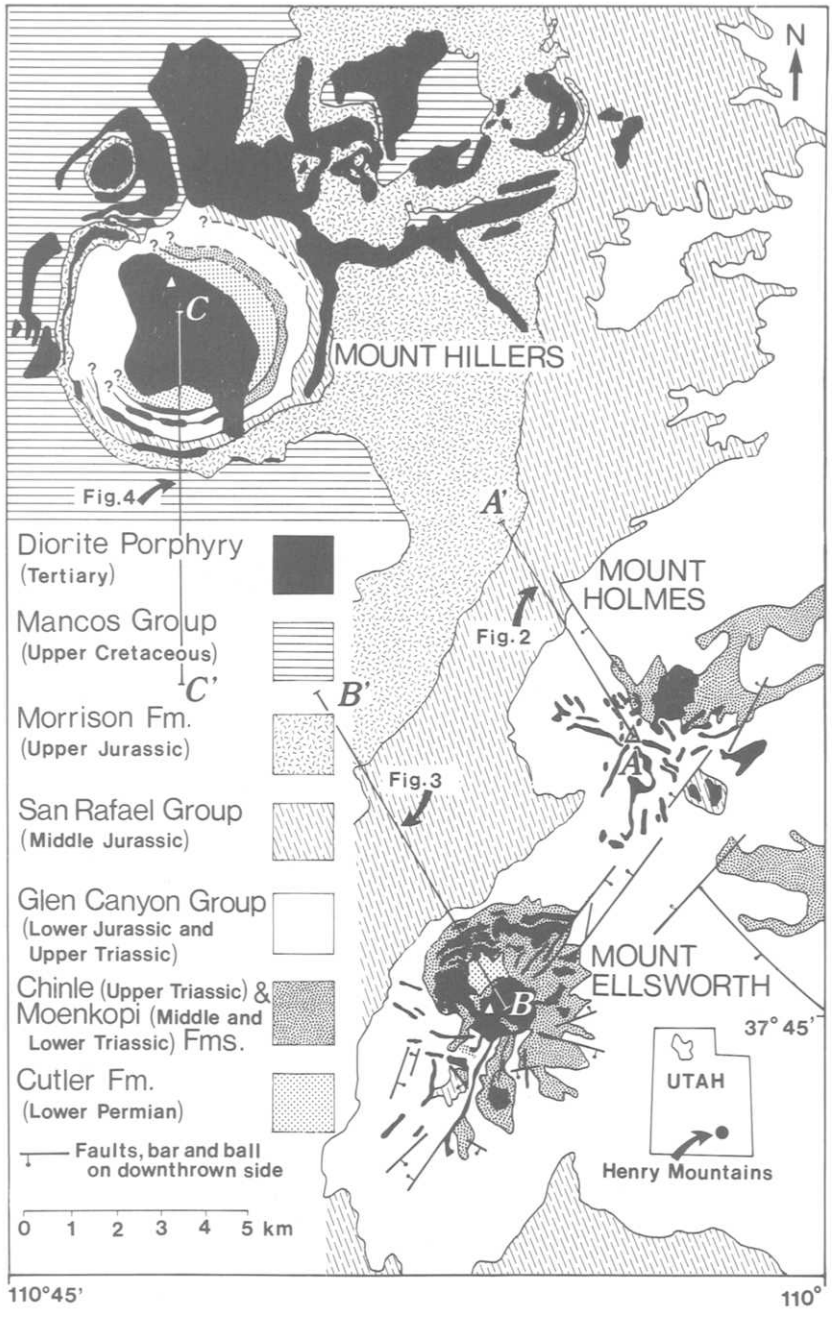

Fig. 1. Simplified geologic map of the southern Henry Mountains (after Hunt 1953 and Jackson & Pollard 1988). Younger rocks crop out progressively from east to west. Open triangles represent mountain summits. Traverses A–A′, B–B′ and C–C′ refer to cross-sections in Figs. 2–4.

used experimental clay models and analysis of the stresses resulting from bending a thick, circular, elastic plate to evaluate the fault patterns that develop in gentle domes of sedimentary rock. Hyndman & Alt (1987) used gelatin models to duplicate the geometry of vertical radial dikes that roll over to feed pancake-shaped laccoliths in the Adel Mountains, central Montana. Dixon & Simpson (1987) showed an evolution of geometric forms undergone by thin, experimental laccoliths, using centrifuge modelling of a stack of paraffin layers. The cover strata above their model intrusions first arched upwards into a sinusoidal, bending shape and, as the overburden above the periphery of the intrusion was abruptly kinked, a cupola form developed. Finally, a flat-topped monocline, similar in shape to the host rock flexures over small laccoliths on the flanks of the Henry Mountain domes, developed as the strata on the flanks of the cupola underwent another episode of localized failure.

Pollard & Johnson (1973) and Koch *et al.* (1981) analyzed the bending of layers over small laccoliths in the Henry Mountains by assuming that the overburden behaves as a stack of elastic layers that slip over one another as they bend in response to pressure in the magma. Although the amplitude of the theoretical bending depends on the total driving force as well as on its distribution, the theoretical flexures all have a simi-

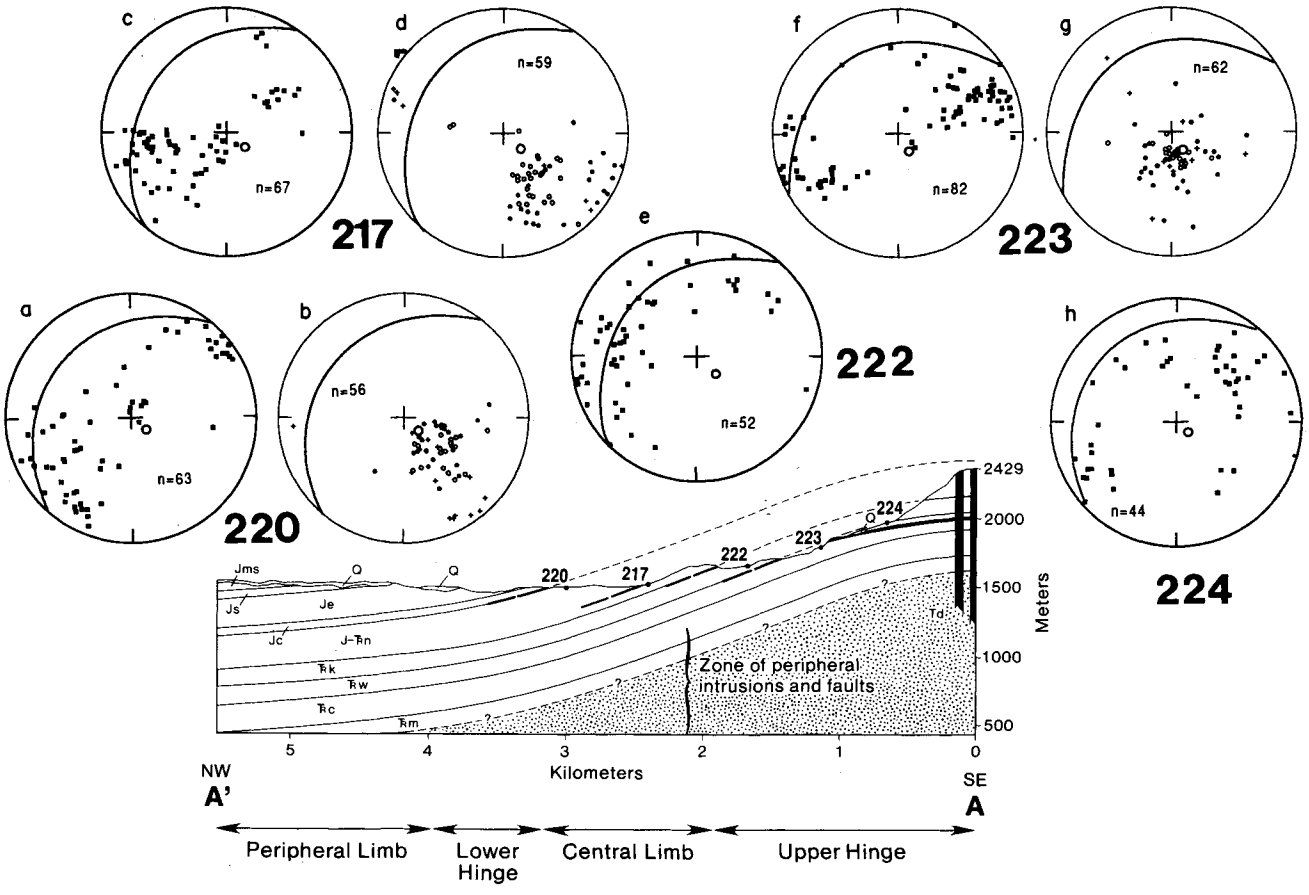

Fig. 2. NW-striking, radially-oriented cross-section and equal-angle stereographic projections of faults at Mount Holmes. Cross-section is based on a laccolithic model of the central intrustion (modified from Jackson & Pollard 1988). The roof–rock contact (drawn at the base of the Triassic section, the deepest rocks exposed on the mountain) is probably much more complex than the concordant shape that we extrapolated from surficial geology. The tapered periphery of the central intrusion represents a zone of satellitic diorite dikes, sills and thin laccoliths distributed through the stratigraphic section. Short heavy lines show locations of bedding-plane fault zones within sandstone units and at formational contacts. Numbers refer to the faulted outcrops described in the text. Q: Quaternary gravels; Kmt: Mancos Shale (Upper Cretaceous), Tununk Member; Kd: Dakota Sandstone (Upper Cretaceous); Jmb: Morrison Formation (Upper Jurassic), Brushy Basin Member; Jms: Morrison Formation, Salt Wash Member; Js: Summerville Formation (Middle Jurassic); Jc: Carmel Formation (Middle Jurassic); Je: Entrada Sandstone (Middle Jurassic); JTrn: Navajo Sandstone (Jurassic and Triassic(?)); Trk: Kayenta Formation (Upper Triassic); Trw: Wingate Sandstone (Upper Triassic), Trc: Chinle Formation (Upper Triassic), Trm: Moenkopi Formation (Middle (?) and Lower Triassic); Pcw: Cutler Formation (Lower Permian), White Rim Member; Pcor: Cutler Formation, Organ Rock Tongue; Pccm: Cutler Formation, Cedar Mesa Sandstone Member. Equal-angle projections: poles to fault planes (solid squares) are shown in (a), (c), (e), (f) and (h). Slickenlines are shown in (b), (d) and (g). Solid circles are normal faults and open circles are reverse faults; crosses represent faults with unknown displacements. Larger open circle denotes pole to bedding and great circle shows the projection of bedding. (a & b) Outcrop 220, Navajo Sandstone. (c & d) Outcrop 217, Navajo Sandstone. (e) Outcrop 222, Kayenta Formation. (f & g) Outcrop 223, Wingate Sandstone. (h) Outcrop 224, Kayenta Formation.

lar, continuous dome-like shape in which the layers are concave-downward over the center and concave-upward over the periphery. This suggests to the above authors that properties of the host rock, such as the presence of bedding-plane faults or differing strengths of the layers, are more important in controlling the shape of the flexures than are the properties of the magma, such as its viscosity and driving pressure distribution. They inferred that the strata should fail initially over the periphery of the intrusions, the site of maximum bending strain and differential stress predicted by the theory. Field observations of peripheral faults, dikes and monoclinal flexures over small laccoliths correlate with these predictions. Pollard & Johnson (1973) and Koch *et al.* (1981) did not identify any bedding-plane faults over the laccoliths in the Henry Mountains, yet such faults are an important element of their theoretical models. For example, if the entire overburden behaved as one layer, 4 km thick and 12 km in diameter, their models predict that the flexural rigidity would have been too great to allow the observed bending.

This paper uses new field observations to describe how faulting accommodated bending and stretching of sedimentary host rocks as the intrusive domes inflated. In particular we describe the geometry and kinematics of deformation accommodated by small, outcrop-scale faults. We use structural data from the faults to estimate directions and relative magnitudes of principal stresses

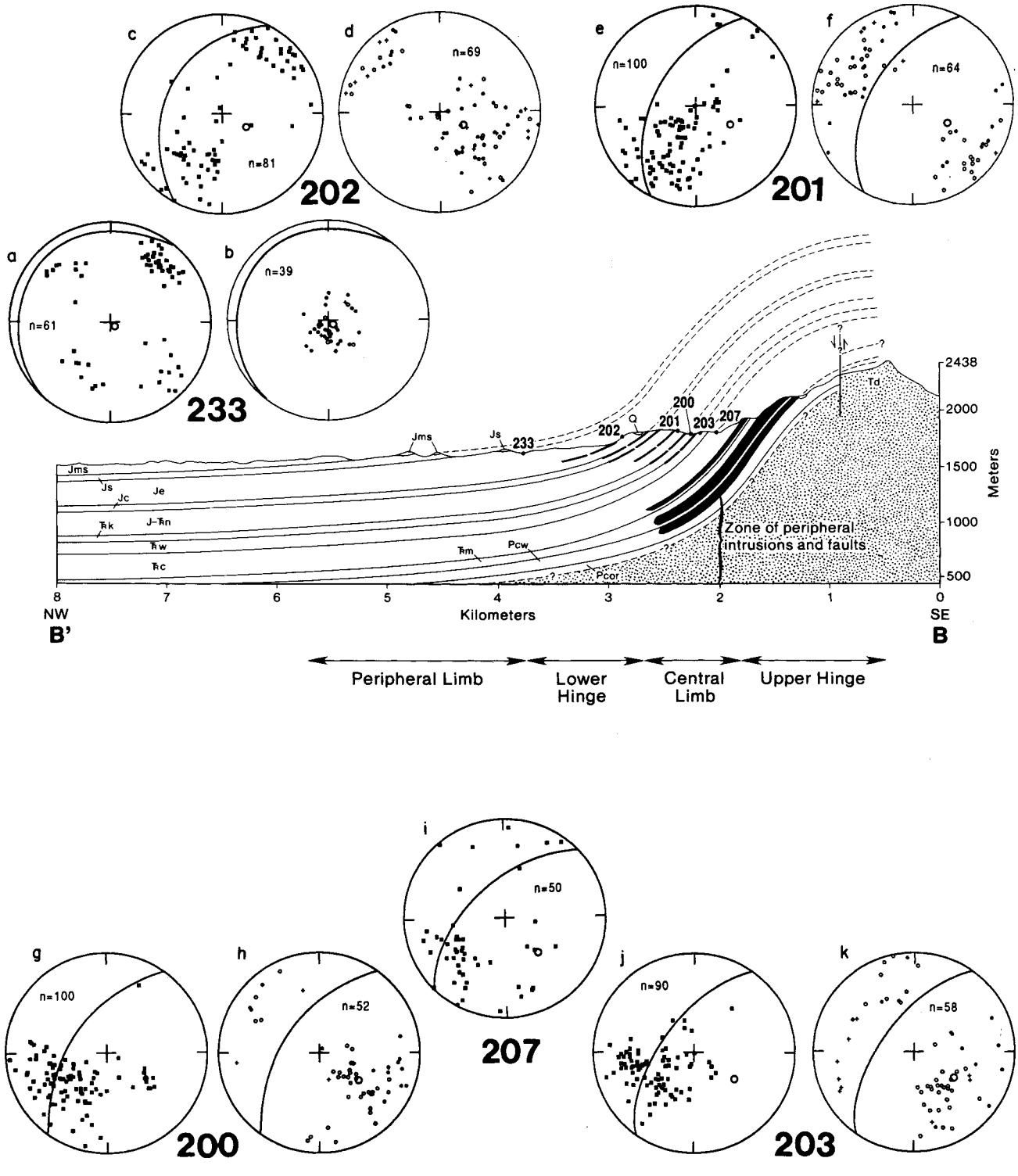

Fig. 3. NW-striking cross-section and equal-angle stereographic plots at Mount Ellsworth. See Fig. 2 for explanation of cross-section. Equal-angle projections: poles to fault planes are shown in (a), (c), (e), (g), (i) and (j). Slickenlines are shown in (b), (d), (f), (h) and (k). Symbols defined in Fig. 2. (a & b) Outcrop 233, Entrada Sandstone. (c & d) Outcrop 202, Entrada Sandstone. (e & f) Outcrop 201, Navajo Sandstone. (g & h) Outcrop 200, Kayenta Formation. (i) Outcrop 207, Moss Back Member, Chinle Formation. (j & k) Outcrop 203, Wingate Sandstone.

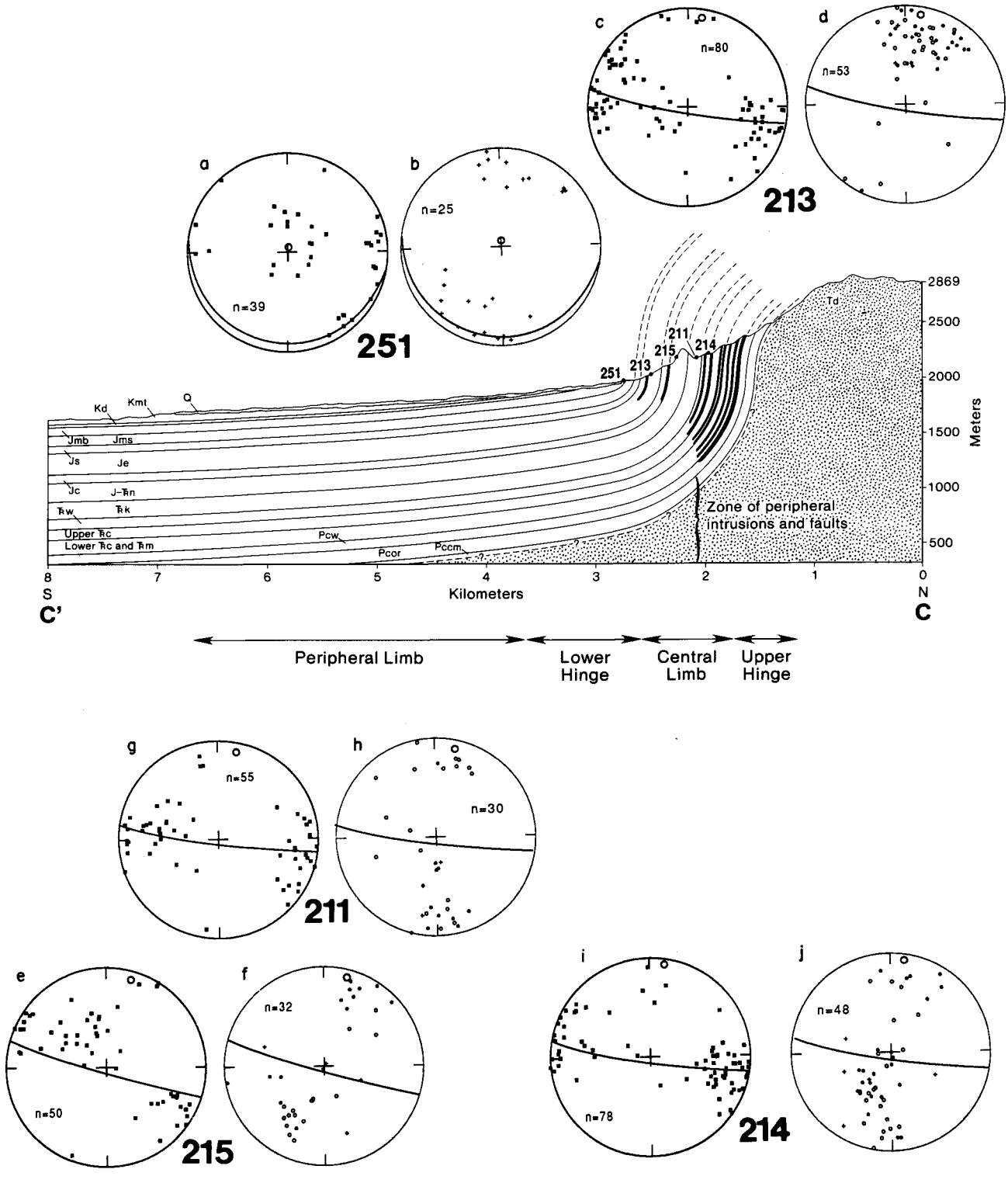

Fig. 4. N–S-striking cross-section and equal-angle stereographic plots at Mount Hillers. See Fig. 2 for explanation of cross-section. Equal-angle projections: poles to fault planes are shown in (a), (c), (e), (g) and (i). Slickenlines are shown in (b), (d), (f), (h) and (j). Symbols defined in Fig. 2. (a & b) Outcrop 251, Dakota Sandstone. (c & d) Outcrop 213, Entrada Sandstone. (e & f) Outcrop 215, Navajo Sandstone. (g & h) Outcrop 211, Kayenta Formation. (i & j) Outcrop 214, Wingate Sandstone.

within the host rock for an early stage of doming, as observed at Mount Holmes. These estimations are compared with the state of stress computed for a bending elastic plate with the same geometry as the mapped flexure. We make a qualitative assessment of the faulting during later stages of doming at Mount Ellsworth and Mount Hillers.

FAULTING IN SANDSTONE LAYERS

Within the domes, faults with both large and small displacements are common and appear to have accommodated much of the host-rock deformation. Shear displacements along map-scale (1 : 24,000) faults with radial and tangential orientations accompanied the deformation at Mount Holmes and Mount Ellsworth, and bound large blocks of flexed host rock (Fig. 1) (see also Jackson & Pollard 1988, figs. 7–9 for more detail). Where measured, the faults have steep, dip-slip displacements of as much as several hundred meters that resulted in upward motion of the central portions of the domes relative to the more peripheral portions. Inwards from the upper hinge of the flexure, the gently-dipping host rock forming the roof of the intrusion is uplifted along many minor faults, commonly occupied by diorite dikes. Displacements perpendicular to the walls of radial diorite dikes accommodated circumferential stretching of the host rock at the summit and flanks of the domes. For example, three diorite dikes 20 m thick radiate from the summit of Mount Holmes. At Mount Ellsworth and Mount Hillers, numerous diorite dikes traverse the crest of the domes, and radial dikes cross-cut older sills on the flanks.

Nature of the outcrop-scale faults

In this paper we focus on outcrop-scale faults with 0.01–1 m offsets. These high-angle faults are most common throughout the sandstone layers of the uplifted strata, from the Salt Wash Member of the Jurassic Morrison Formation to the Moss Back Member of the Triassic Chinle Formation (proceeding from the distal to the proximal part of the domes; Figs. 2–4). The faults are best exposed in the central limbs of the flexures. Individual faults range from less than 0.5 mm to greater than 1 cm in width and crop out as steeply-dipping normal and reverse faults. The faults contain fillings of crushed sandstone that occasionally exhibit new growths of quartz (Fig. 5a) and strike at high angles to the beds, in orientations that are roughly symmetric about the radial planes of the domes (Jackson 1987, p. 123). The local spacing of the faults ranges from centimeters to several meters. The strong radial symmetry of the faults about each of the domes suggests that the faults formed during flexure of the strata; they are not related to the NW-striking joints in the plateaus adjacent to the domes. In formations composed of shales or mudstones and in the deeper Permian strata at Mount Hillers, which have suffered contact metamorphism, the small faults are less common. An unknown amount of more pervasive grain-scale deformation accommodated strains within these layers.

The small faults resemble deformation bands and zones of deformation bands described by Aydin (1978) and Aydin & Johnson (1987) in the Entrada and Navajo Sandstones in the nearby San Rafael desert. Thin sections of deformation bands from the Henry Mountains reveal zones of crushed and consolidated sandstone about 1–1.5 mm thick. The inner zone is composed of angular fragments of sand grains, with much smaller grain size, poorer sorting and lower porosity than the host sandstone (Aydin 1978). Relative to the intensity of deformation along the small faults, the sedimentary textures of the host sandstones are almost undisturbed. At Mount Hillers, however, where the host-rock deformation is the most pronounced, the sandstones locally show such features as calcite twins, mutual interpenetration of quartz grains and some 120° grain-boundary intersections, suggesting recrystallization of the sandstone.

Outcrop lengths of the faults range from a few meters to several tens of meters. Most faults are composed of echelon segments, tens of centimeters to many meters in length. Linkage occurs with motion along individual segments and produces a slightly wavy form to the fault planes when viewed on outcrops oriented normal to the fault plane and containing the slip direction. At points where the echelon segments link to form longer faults, secondary splay fractures propagated into the intact sandstone. Offsets among the faults are complex (Fig. 5a) and indicate that slip on faults with similar orientations can be separated in time by slip on members of a different set at the same locality. Because the faults intersect one another at varying angles, and because splay fractures have developed at the linkages of many segments, most fault networks have a complicated outcrop pattern (Fig. 5b).

At Mount Holmes, Mount Ellsworth and Mount Hillers (Fig. 1), we measured samples of the small faults along radial traverses that approximately parallel the radial cross-sections shown in Figs. 2–4. The purpose of the measurements was to identify families of faults, to establish the relative timing of slip along the faults, and to discover how these faults accommodated deformation during growth of the dome. Only the faults containing resistant fillings, slickensides and/or measurable shear offsets were measured. Field measurements included the fault-plane attitude, slickenline attitude, sense of relative movement (hanging wall up or down) and offsetting relationships with other faults.

Slickenlines are expressed as faint, black streaks within light-colored fault fillings, and as grooves within the fault surface that commonly parallel the streaks. Offset sedimentary layering, cross-beds and other faults demonstrate that the shear displacement across most of the small faults is a few millimeters to a few centimeters (Fig. 6). Less commonly, displacements are several centimeters and, rarely, 1 or 2 m. At Mount Ellsworth

(a)

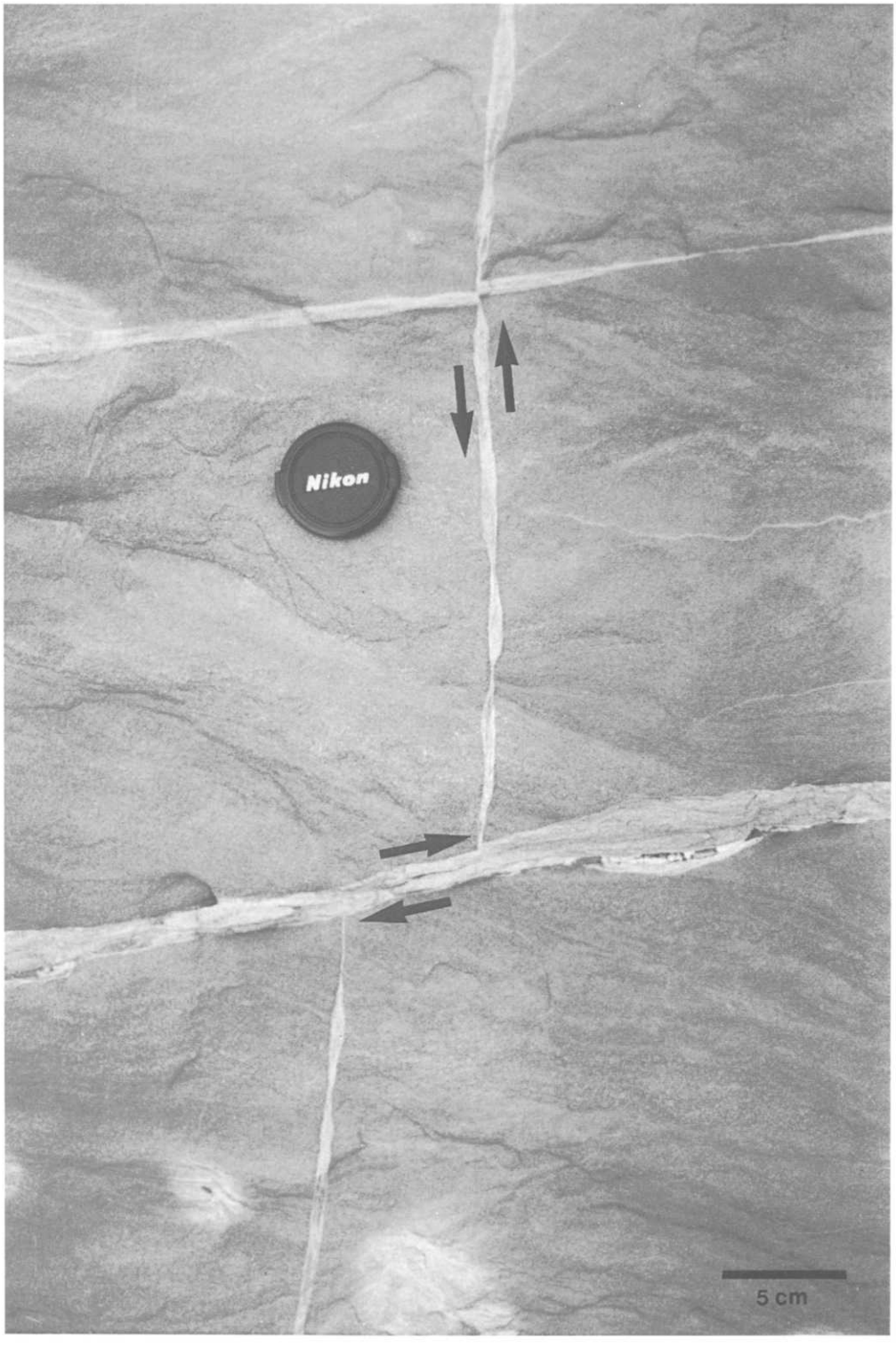

Fig. 5. Photographs of high-angle outcrop-scale faults or deformation bands (Aydin 1978). (a) Offsets among faults, Entrada Sandstone, outcrop 203, Mount Ellsworth. The faults are formed of zones of deformation bands, which contain thin fillings of crushed sandstone.

(b)

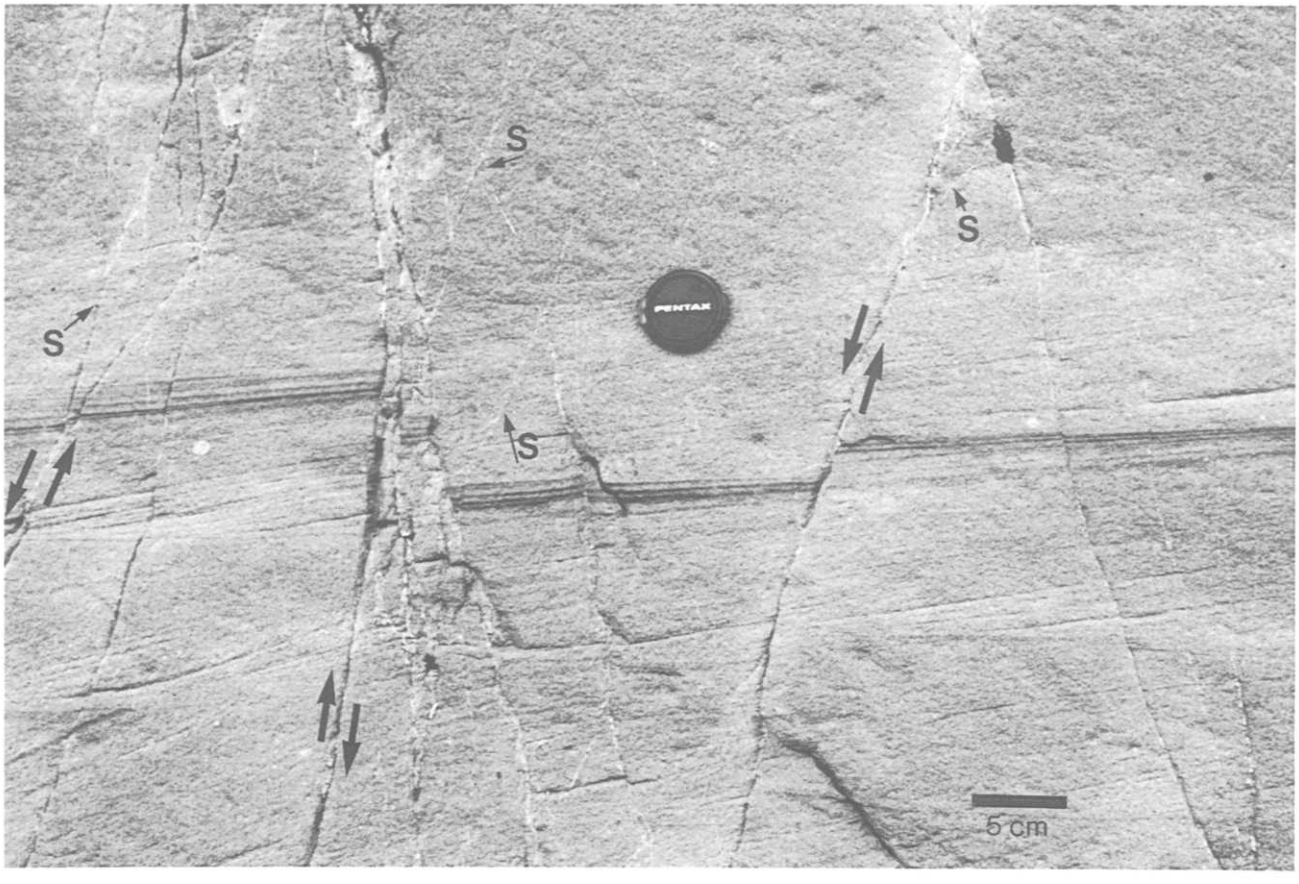

Fig. 5. *continued* (b) Network of faults within the Kayenta Formation, outcrop 200, Mount Ellsworth. Many splay faults (shown by S) diverge from the primary fault planes.

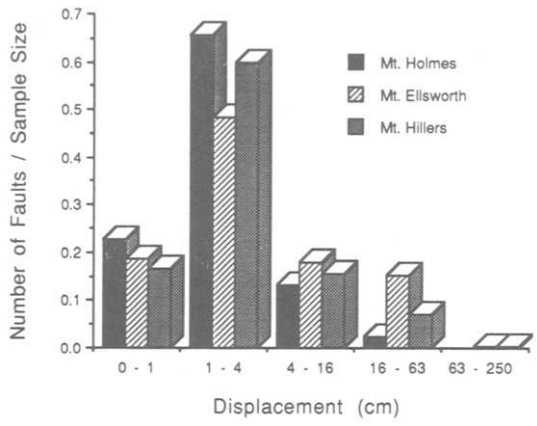

Fig. 6. Plot of displacement and proportion of faults with that displacement, for fault samples at Mount Holmes ($n = 263$), Mount Ellsworth ($n = 378$) and Mount Hillers ($n = 218$).

and Mount Hillers, faults with 4–63 cm of displacement form larger proportions of the populations than at Mount Holmes. Displacements at Mount Hillers are not substantially larger, however, despite the increased vertical deflection of the strata. This suggests that some other process, probably solid body rotation of the beds, accommodated part of the deformation in the more advanced stages of doming.

Within the central limbs of the flexures, thin fault surfaces containing light-colored resistant fillings of crushed sand grains occur at most formational contacts and along the truncating surfaces of large aeolian dunes within sandstone units, such as the Entrada and Navajo Sandstones. Within the gently-dipping (20°) central limb of the flexure at Mount Holmes, bedding-plane faults are exposed at the Navajo–Carmel contact, at two horizons within the Navajo Sandstone, at the Navajo–Kayenta contact, and at the Kayenta–Wingate contact (Fig. 2). The typical spacing of these zones is less than 200 m, measured perpendicular to the beds. At some localities, these bedding-plane faults form zones less than 1 m thick, consisting of several thin gouge surfaces bounding a complicated network of cross-faults. The spacing of these faults is taken to define the thickness of mechanical layers within the flexures. Minor bedding-plane faults, composed of a single thin deformation band, occur between the thicker zones. Because of the lack of marker planes crossing the bedding-plane faults, the magnitudes of shear displacements are not known. Orientations of the bedding-plane faults and associated slickenlines, measured along a radial traverse at each flexure, are shown in Fig. 7. In general, the bedding-plane faults strike tangentially to the domes and display oblique-slip motions, often with a large component in the radial direction of the dome.

THE EARLY STAGE OF DOMING

Gilbert (1877, pp. 74–77) proposed that deformation over the Henry Mountains intrusions involved flexure of host-rock layers, at least in the early stages of doming. The cross-sections (Figs. 2–4) illustrate where hinges developed at the crests and peripheries of the southern Henry Mountain domes. Bedding-plane fault zones found within sandstone units and formational contacts (Figs. 2, 3 and 7) indicate that the overburden behaved as a stack of mechanical layers able, at least in some places, to slip over one another. Jackson & Pollard (1988) hypothesized that large stresses developed before the initiation of doming, when the overburden behaved as a single, 4 km thick mechanical layer, loaded at its base by the magma pressure in a sill. These authors suggested that slip along bedding-plane faults relieved these stresses and reduced the effective mechanical thickness of the overburden, greatly reducing the flex-

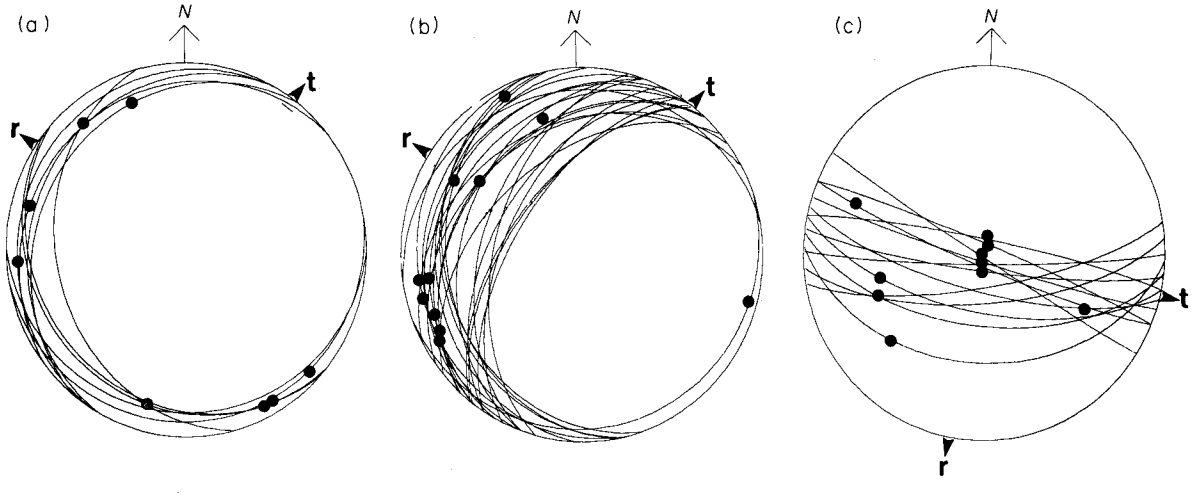

Fig. 7. Equal-area stereographic projections of bedding-plane faults with their representative slickenlines along radial traverses through the flexures. (All stereographic plots in this paper are lower-hemisphere projections.) Radial and tangential co-ordinate directions of the dome are shown by r and t. (a) Faults within the lower hinge and central limb of the flexure, Mount Holmes. Nine measurements. (b) Faults within the lower hinge and central limb of the flexure, Mount Ellsworth. Twenty-five measurements. (c) Faults within the central limb of the flexure, Mount Hillers. Thirteen measurements. Fewer bedding-plane faults were measured at Mount Hillers because of smaller outcrop areas and rough terrain.

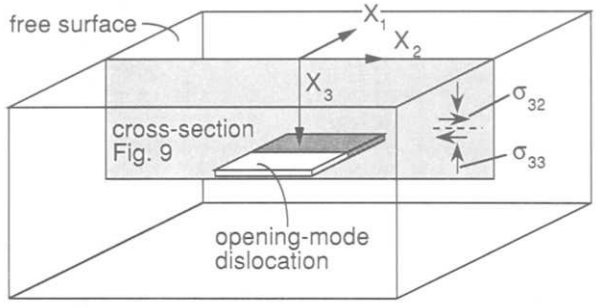

Fig. 8. Definition sketch of a square, pure opening-mode dislocation showing X_1, X_2, X_3 co-ordinate directions.

ural rigidity of the overburden and, thereby, permitting growth of the domes. For typical spacings of 150–200 m between bedding-plane faults at Mount Holmes, Jackson & Pollard (1988, p. 134) suggested that the sill–laccolith transition radius, the radius at which symmetric displacements above and below a sill give way to significant flexure of the overburden and thickening of the laccolith, would be at least 1.1 km.

To evaluate the tendency for slip on bedding planes above a sill and the likely locations of such faults, we follow Erickson (1987). We compute the distribution of normal and shear stresses (Fig. 8) acting on horizontal planes over an opening-mode dislocation at 4 km depth in a linear elastic half-space that is homogeneous and isotropic with respect to elastic moduli. This analysis neglects differences in elastic moduli among the lithologic units in the Henry Mountains that could contribute to a somewhat different flexural rigidity of the overburden (Pollard & Johnson 1973). It is implicit that horizontal planes (bedding surfaces) are weak and would slip in preference to non-horizontal planes carrying a greater shear stress and/or lesser normal stress. The stress analysis does not explicitly include these bedding-plane faults and so can only address their potential for formation.

The plan shape of the dislocation is square, to approximate a circular sill. The 'radius' is taken as the half-length of the square, and the 'X_2X_3' plane is taken as a representative cross-section. Assuming no ambient shear stress on horizontal planes, the shear stress, σ_{32}, induced by the dislocation is solely responsible for driving slip. Slip would be resisted by the effective normal stress, σ_n which is composed of stress induced by the dislocation, σ_{33}, plus the assumed lithostatic stress, $\rho_r g X_3$, minus the assumed hydrostatic pore pressure $\rho_w g X_3$. The tendency for slip on horizontal planes is measured by $F = |\sigma_{32}| - \mu[\sigma_{33} + (\rho_r - \rho_w)gX_3]$ (Segall & Pollard 1980, Oppenheimer *et al.* 1988), where $(\rho_r - \rho_w) \simeq 1.4 \times 10^3$ kg m^{-3} and $\mu \simeq 0.85$ is the coefficient of friction (Byerlee 1978). For negligible cohesion, when $F > 0$ the frictional strength across horizontal planes is exceeded and we would expect slip. For non-negligible cohesion, F must exceed the cohesive shear strength.

Figure 9 shows contour plots of the slip tendency, F, around dislocations with constant thicknesses that are 1/100 of their radius. For a 0.5 km radius and 5 m thickness (Fig. 9a), F is large enough to cause slip only near the tip of the dislocation. Thus, we would expect intrusions of this dimension to remain as sills. Except in the immediate vicinity of the dislocation, only negligible normal and shear stresses are induced on horizontal planes, and the negative product of the friction and the 'effective' lithostatic compressive stress, $-\mu[(\rho_r - \rho_w)gX_3]$, shown by the subhorizontal −25 and −50 MPa contours, remains essentially unchanged. As the dislocation grows to a thickness of 10 m and a radius of 1 km (Fig. 9b), the region of potential slip begins to extend upward through the overburden and downward from the free surface. At a radius of 1.5 km (Fig. 9c), the minimum radius predicted by Jackson & Pollard (1988, p. 134) for sill–laccolith transition in the southern Henry Mountain domes, the slip region extends through the entire overburden. At 2 km radius and a 20 m opening displacement, the potential slip region has spread to a radius of about 4 km and would encompass much of the long peripheral limb of the host-rock flexure (Jackson & Pollard 1988, p. 133). We expect no bedding-plane faults to form above the central portion of the intrusion, where vertical compressive stresses are greatest. For elevated pore pressures or a lower friction coefficient, the tendency to slip would spread through the entire 4 km thickness of sedimentary host rock at radii less than 1.5 km.

The mechanical analysis demonstrates that bedding-plane faults could have developed through the entire overburden thickness. Our observations and this analysis support the hypothesis that the bedding-plane faults accommodated flexure of the strata by subdividing the overburden into thinner mechanical layers that slipped over one another. In addition, the shale layers that are interleaved between thick sandstone formations probably accommodated an unknown amount of shear deformation; no cleavage, however, is developed in these beds.

STRESS DURING THE FLEXURAL STAGE OF DOMING

In addition to the bedding-plane faults, networks of small faults that strike at high angles to the beds were active within the central limb and hinges of the flexure at Mount Holmes. In this section, we analyze the relative movements of these high-angle faults to evaluate whether they relieved strains at the tops and bottoms of the mechanical layers, where bending strains are theoretically at a maximum. A strong radial symmetry of outcrop-scale faults around all three domes and a lack of tectonic structures away from the intrusive centers indicate that the faults are related to the doming. Furthermore, within certain outcrops at Mount Holmes, populations of reverse, normal and oblique-slip faults coexist. On the basis of this spatial and geometric association between faulting and doming, we postulate that the ambient state of stress that existed just before flexure did not deviate dramatically from Anderson's (1951) isotro-

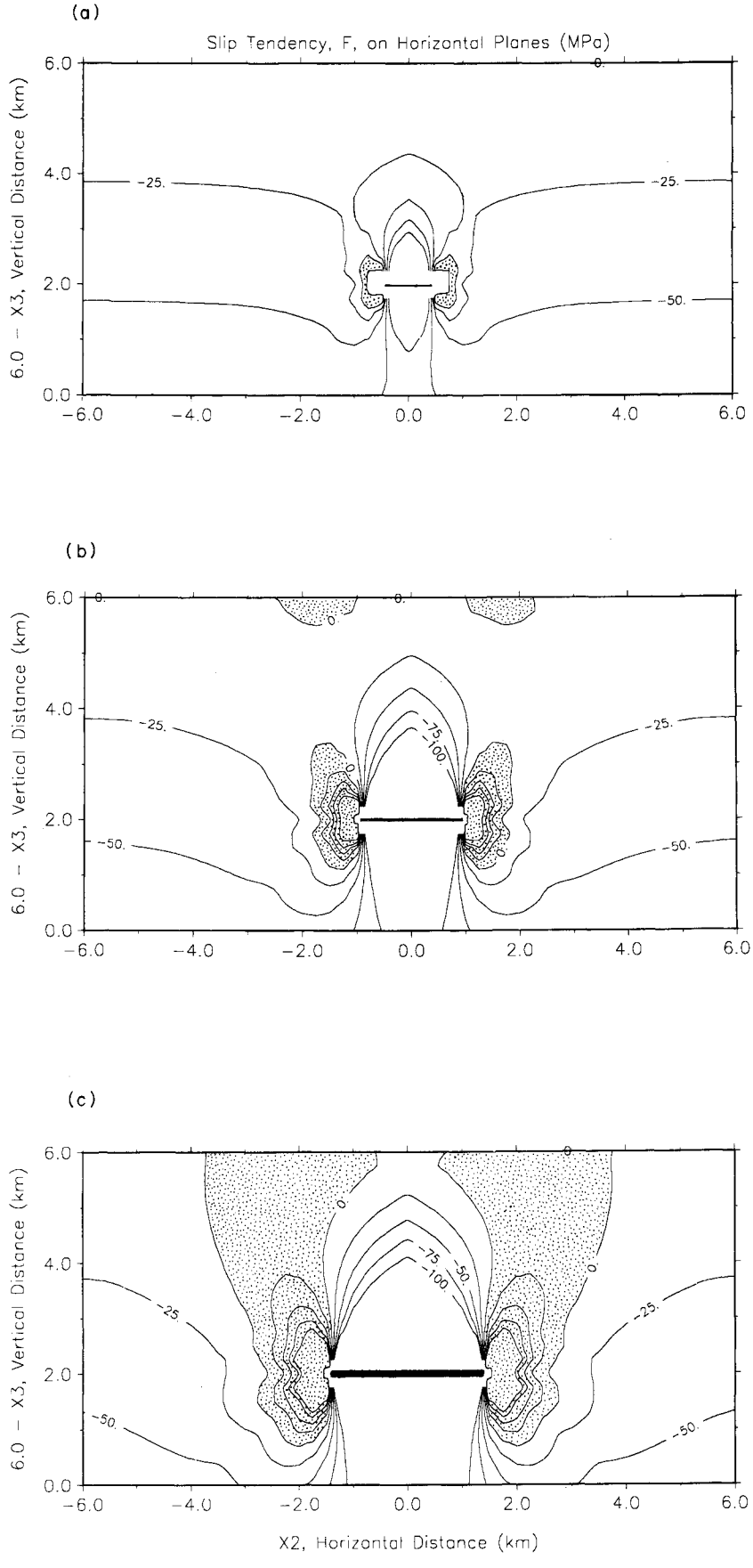

Fig. 9. Contour plots of slip tendency, F, in MPa, on horizontal planes over opening-mode dislocations (solid heavy lines) at 4 km depth. Stippled areas are regions of potential slip, where $F > 0$, on horizontal planes. (a) A 5 m thick dislocation 0.5 km in radius. (b) A 10 km thick dislocation 1.0 km in radius. (c) A 15 m thick dislocation 1.5 km in radius. Contours of frictional driving stress magnitudes < -100 MPa and > 100 MPa are not shown. A region of high negative values of F lies beneath the dislocations; bedding-plane slip is unlikely there. High positive values of F at the dislocation tips suggest a much greater likelihood of slip in these regions.

pic standard state. If large stress differences had been present, they would have disrupted the radial symmetry and biased the faulting to one type. We estimate that about 3 km of sedimentary rock with an average density of 2.4×10^3 kg m^{-3} overlay the faulted outcrops, so the magnitude of this lithostatic compressive stress was $\sigma_a \sim 70$ MPa.

Fault-population orientation data

At Mount Holmes, we measured five samples of 50–100 faults along a NW-trending radial traverse, which roughly parallels the NW-striking cross-section (see Figs. 1 and 2 for outcrop locations). The following section describes orientation data from fault samples measured within the Jurassic and Triassic sandstones, beginning with the most peripheral outcrops. Beds dip about 20° in this part of the flexure.

We measured samples of small faults in the Navajo Sandstone (outcrops 220 and 217) at the transition from the lower hinge to the central limb and within the central limb of the flexure (Fig. 2). Outcrop 223 lies within the Wingate Sandstone at the transition from the central limb of the flexure to the upper hinge. Those within the Kayenta Formation (outcrops 222 and 224) are located in the central limb and upper hinge. The greatest density of faults occurs near bedding-plane fault zones; the sandstone is cut by few, or no, faults at the center of some mechanical layers. Within the Navajo and Wingate Sandstones the faults strike within 50° of the radial direction and dip to the NE and SW (Fig. 10). These are left and right lateral oblique-slip faults, which mutually offset one another with no consistent pattern.

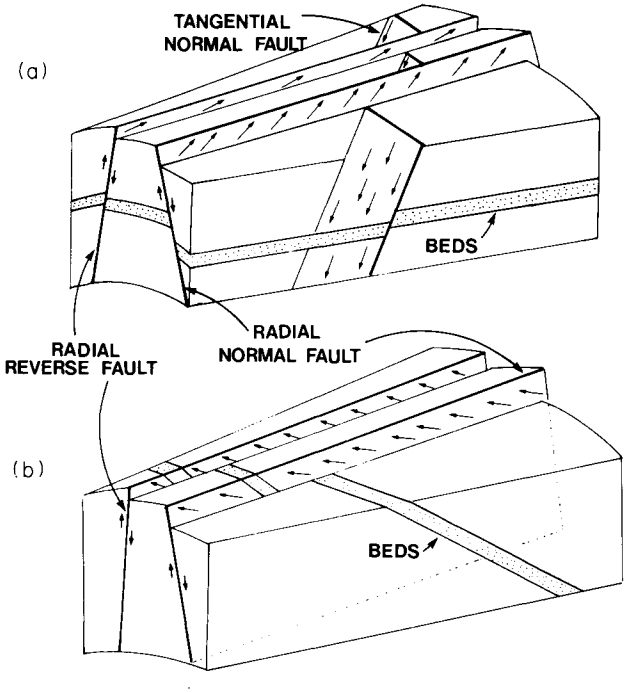

Fig. 10. Block diagrams illustrating typical fault orientations. (a) At Mount Holmes, beds dip gently and high-angle faults have slickenlines that plunge in the same general direction as the bed normal (to the SE). Rare tangentially striking high-angle faults have normal or reverse displacements. (b) When the doming is more advanced and the beds dip more steeply, as at Mount Ellsworth and Mount Hillers, slickenlines plunge in the direction of the bed normal (as in a) and, also, approximately parallel to the dip direction of the beds.

At the most distal Navajo outcrop (220), slickenlines on the sub-radially oriented faults plunge between 60° and 22° SE, giving predominantly oblique-slip normal and reverse faults (Figs. 2a & b). The faults at the more proximal Navajo outcrop (217) dip less steeply and have slickenlines that plunge between 53° and 2° SE, giving oblique-slip and nearly strike-slip faults (Figs. 2c & d). At the Wingate outcrop (223) slip directions vary from nearly radial to tangential orientations. These slickenlines plunge between 70° and 35° SE (Figs. 2f & g). Slip directions at the three outcrops show the following pattern: nearly all the slickenlines are contained within the SE quadrant of the stereonet; normal and reverse displacements have similar orientations, and nearly all the slickenlines record oblique-slip motions on the fault planes.

Fault samples measured at two localities within the Kayenta Formation (Fig. 2) show somewhat different orientation patterns. Bedding-plane faults are rare or absent at these outcrops. The outcrop located within the central limb of the flexure (outcrop 222) has normal and reverse faults that strike at high angles to the beds and dip to the NE and SW (Fig. 2e); the rare slickenlines that are exposed plunge to the SSE. In addition, many tangentially-striking reverse faults dip steeply towards the central intrusion. In the Kayenta Formation exposed within the upper hinge (outcrop 224), the beds dip 14°. Both the high-angle faults and tangentially-striking faults have predominantly normal displacements (Fig. 2h). Few slickenlines are exposed.

Elastic plate theory

At Mount Holmes, limb dips within the flexure are gentle—less than about 20°. The mechanical layers apparently had thicknesses of about 200 m and were bent over a radius of about 4 km, so they had very small thickness to length ratios. In addition, the layer deflection based on the shape of the Navajo Sandstone in cross-section (Fig. 2) and expressed over the radius over which bending is concentrated (about 4 km) is quite similar to the deflection shape predicted by elastic plate theory (Jackson & Pollard 1988, Fig. 17). In these respects, doming of the overburden at Mount Holmes may be approximated by elastic plate theory for the bending of a stack of thin elastic plates that have slipped over one another (Timoshenko & Woinowsky-Krieger 1959, pp. 55–56).

The doming at Mount Holmes was complicated by frictional resistance to sliding so that layer-parallel shear stresses were transmitted across the bedding-plane faults. In addition, the radial cross-section indicates that the layers suffered a radial extension of as much as 4% (Jackson & Pollard 1988). Despite these departures from ideal behavior, we compare principal directions of stress computed from samples of faults with those predicted by elastic plate theory in the spirit of seeking the simplest explanation for the flexures. We then evaluate

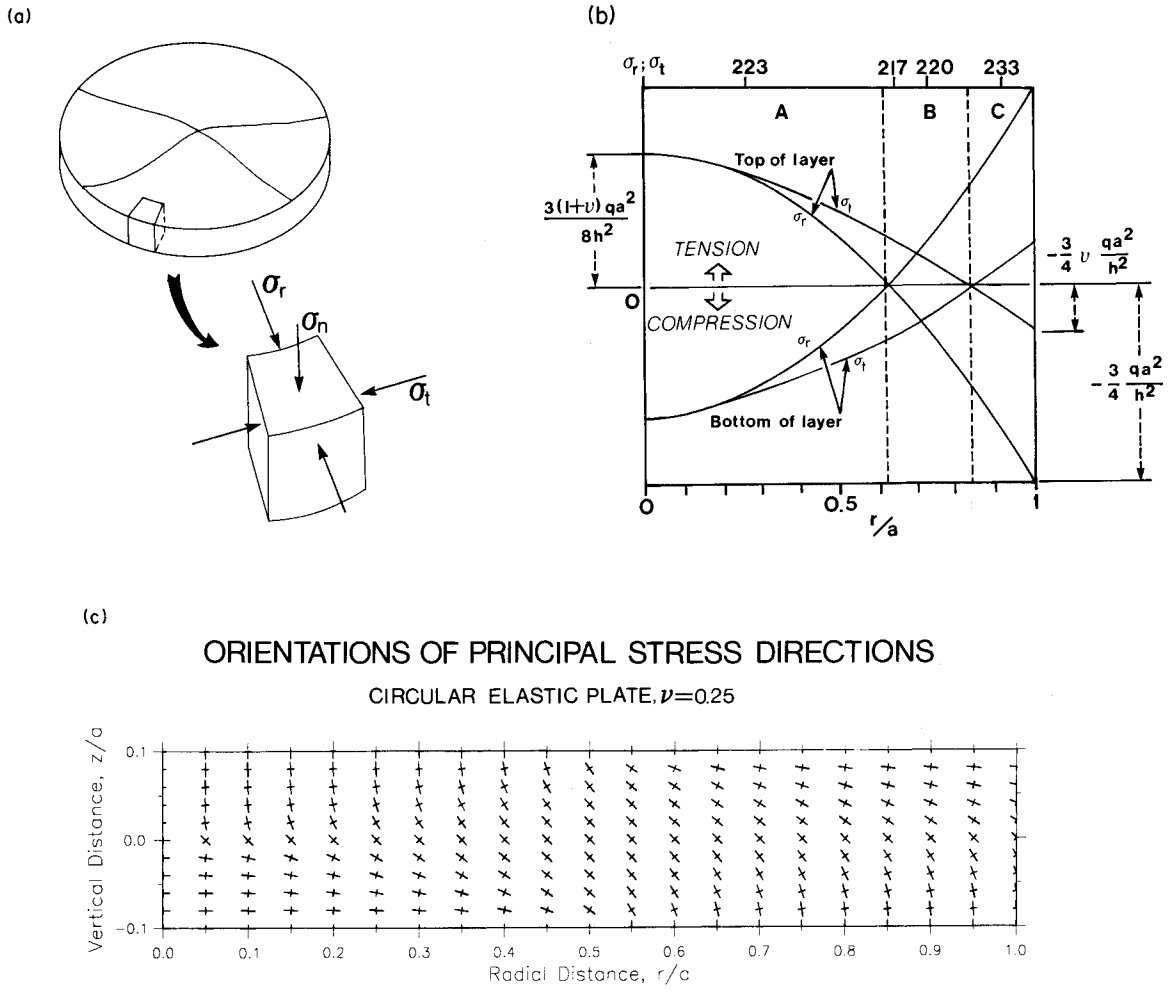

Fig. 11. (a) Definition sketch of a circular bending plate showing the orientations of the layer-normal (σ_n), radial (σ_r) and tangential (σ_t) components of stress. (b) Variation in relative magnitudes of horizontal principal stresses along the radius of a thin, circular bending plate. Layer is concave-downward over zone A and concave-upward over zone C. Curves show the variation in relative magnitudes of tangential (σ_t) and radial (σ_r) stresses at the top and bottom surfaces of the plate. At most, stresses do not differ in magnitude by more than a factor of Poisson's ratio. The relative locations of outcrops 233, 217, 220 and 223 are shown. (c) Orientations of principal stress directions σ_1 and σ_2 in a bending layer. Short lines: most compressive principal stress. Long lines: least compressive principal stress.

the relative importance of bending stresses, layer-parallel shear and tension resulting from layer stretching at different points within the flexure.

For a single elastic plate (Fig. 11a), one component of the stress change due to flexure, σ_n, is directed perpendicular to the surface of the layer and has a magnitude equal to zero. That is, it is unchanged by flexure. The other two components of the stress change act in the radial, σ_r, and tangential, σ_t, co-ordinate directions. These stress changes must be added to the ambient stress, σ_a, to give the complete state of stress. The boundary conditions of the plate model specify that the shear stress is zero along the top and bottom surfaces of the plate. This condition would be approximately obtained in the domes if the bedding-plane faults slipped enough to reduce the shear stress on the layer boundaries to a small fraction of the bending stresses within the layers. At the upper and lower boundaries of the plate, σ_n, σ_r and σ_t are coaxial with the principal directions of stress. However, which co-ordinate direction (normal, radial or tangential) corresponds to which principal stress (σ_1, σ_2 and σ_3) depends upon position in the layer.

At the top and bottom of the plate, the variation in the magnitudes of σ_r and σ_t (Fig. 11b) defines three distinct deformational zones (Timoshenko & Woinowsky-Krieger 1959, pp. 55–56). These correspond to the concave-downward hinge within the crest of the dome, the central limb and the concave-upward hinge at its periphery. Near the crest of the dome in zone A the two stress components are equal in magnitude, and both are tensile at the top of the layer and compressive at the bottom. In zone B, the stresses are smaller in magnitude–one is tensile and the other is compressive. Near the periphery of the dome in zone C, both stresses are compressive at the top of the layer, and the radial compression is greater than the tangential compression. At the bottom of the layer, both stresses are tensile, and the radial tension exceeds the tangential tension. Plate theory predicts that σ_r and σ_t do not differ by more than a

factor of Poisson's ratio, which has a value of 0.1–0.3 in a selection of porous sandstones (Clark 1966).

Components of stress change (σ_n, σ_r) are not coaxial with the principal stresses near the middle plane of the layer, where the principal stress directions are steeply inclined (Fig. 11c). In this region, however, the bending stresses are small and would be less likely to induce faulting. At Mount Holmes, the high-angle faults seem to be concentrated near the bedding-plane fault zones; therefore, we will focus only on the stress changes near the top and bottom surfaces of the layer (Fig. 11b).

Table 1. Stress notations

σ_a	Ambient stress magnitude, postulated to be approximately isotropic
σ_n, σ_r, σ_t	Components of normal stress change due to bending; co-ordinate directions are n (layer normal), r (radial) and t (tangential)
σ_1, σ_2, σ_3	Principal stresses; $\sigma_1 \geq \sigma_2 \geq \sigma_3$
S_1, S_2, S_3	Deviatoric principal stresses computed from fault data; any deviatoric component of σ_a in included in S_{ij}

Faulting theory

We use the fault orientations and slip directions at three outcrops from Mount Holmes and one from the periphery of Mount Ellsworth, where the deformation is least advanced, to estimate the orientations and relative magnitudes of the principal stresses associated with the faulting. These estimated states of stress are compared to stress states (Fig. 11b) calculated for circular elastic plates bent into configurations similar to the flexed layers of the domes (Jackson & Pollard 1988, fig. 17).

Techniques developed by Angelier (1979), Michael (1984) and Reches (1987) compute the deviatoric stress-tensor that minimizes the difference between the measured slip direction and the estimated shear stress direction on a variety of fault planes within a region. Because the method assumes that the deviatoric stress is homogeneous within the outcrop being studied and constant for the duration of the faulting events, its validity depends upon all slip events being independent and driven by the same stress tensor. Only the relative magnitudes of the principal stresses (S_1, S_2, S_3) of the deviatoric stress tensors are computed. These must be coupled with the isotropic components of both the ambient and flexural stress states to determine the total state of stress.

Michael's (1984) method computes the tangential traction, or maximum shear stress acting on a variety of planes within a region by subtracting the normal traction from the total traction acting on each of these planes. To accomplish this, two assumptions are made (and later tested with error computations). First, the direction of the shear traction vector, $\boldsymbol{\tau}$, is assumed to parallel the slip direction, $\boldsymbol{s}$. Second, the magnitude of the shear traction, $|\boldsymbol{\tau}|$, is assumed to have a similar value on all fault planes at the time of rupture. This is physically appealing in that one might suppose that the shear strengths of all the fault planes were similar. Because only the relative magnitudes of the deviatoric stress tensor elements are found, this assumption is expressed as $|\boldsymbol{\tau}| = 1$. With these assumptions, the components of the tangential traction vector can be described in terms of the fault normal, slip direction and deviatoric stress components. The principal stress components are the same, but unknown for every fault. The single stress tensor that best satisfies all the faults is found by solving a system of linear equations and the error limits for the principal directions are estimated using linear least-squares techniques. After the stress tensor that represents the best fit to the data is computed, the tangential traction acting on each of the fault planes is calculated and compared to the measured directions of slip. The average angle between these two vectors, $\bar{\beta}$, should ideally be close to zero, but we accept values up to 20° as being instructive of the state of stress. The average value of the magnitude of the shear traction vector on all the faults, $\bar{\tau}$, should ideally be close to unity; when $\bar{\tau}$ ranges from 0.80 to 1.0, the fit of the stress tensor to the measured data is considered good. The parameter $\phi = (S_2 - S_3)/(S_1 - S_3)$ is a measure of the relative magnitudes of the deviatoric principal stresses, where S_1, S_2 and S_3 (Table 1) are the principal stresses ordered from most compressive to most tensile.

Stress analysis results

We analyzed fault samples from the upper hinge of the flexure at Mount Holmes (outcrop 223; see Figs. 2 and 3 for locations), the central limb at Mount Holmes (outcrop 217), the transition from the central limb to the lower hinge of the flexure at Mount Holmes (outcrop 220) and the periphery of the flexure at Mount Ellsworth (outcrop 233). The normalized radial positions of these outcrops are plotted in Fig. 11(b). Here, the radial distance a is the radius over which the curvature of the beds is significant (Jackson & Pollard 1988, fig. 14); $a = 4$ km at Mount Holmes and $a = 3.3$ km at Mount Ellsworth.

Crest of the flexure, Mount Holmes. At the transition from the central limb to the upper hinge of the flexure at Mount Holmes, sub-radially and obliquely-striking normal faults and fewer reverse faults cut the upper portion of the Wingate Sandstone, which dips about 19° NW (outcrop 223; Figs. 2f & g and 12). A few thin bedding-plane faults are distributed throughout the outcrop, but the quality of exposures does not allow the independent location of the outcrop relative to the top or bottom of a mechanical layer. The preponderance of normal faults, however, suggests proximity to the top. The fit of the entire population of 46 normal and reverse faults to a single stress tensor (Fig. 12) is poor ($\bar{\beta} = 39°$, $\bar{\tau} = 0.62$), indicating that the state of stress may not have remained consistent for the duration of faulting. Anderson's (1951) theory of faulting suggests that it would be unlikely that one state of stress should be associated with

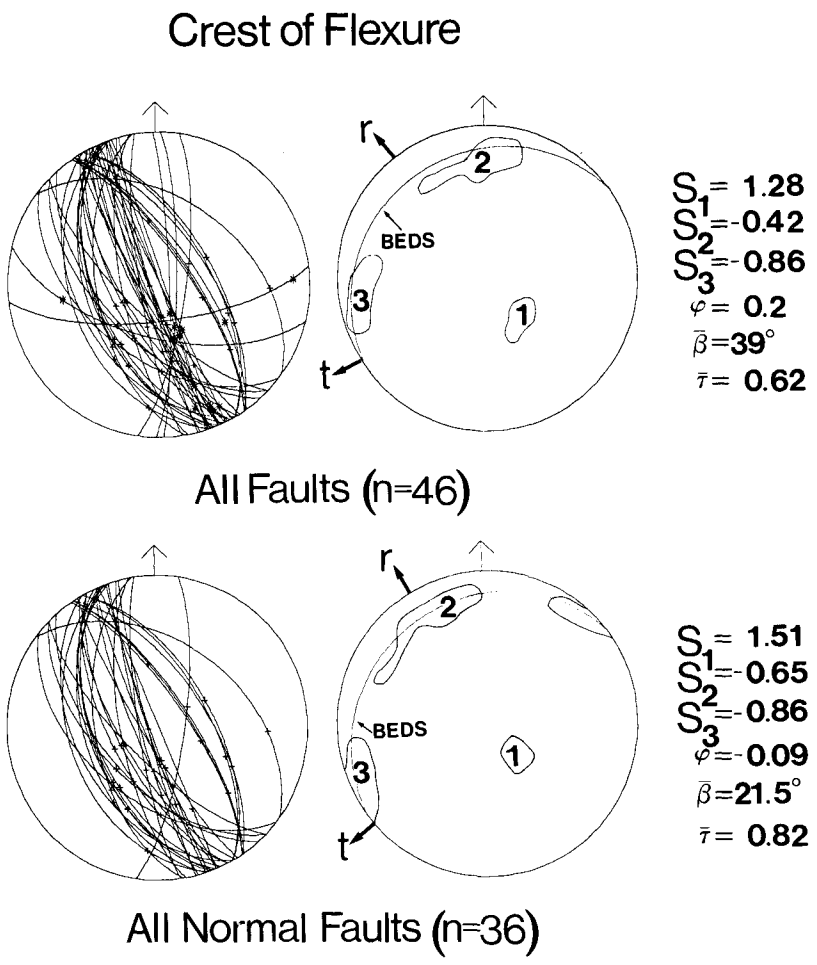

Fig. 12. Fault data and computed stress axes at the transition from the central limb of the flexure to the upper hinge at Mount Holmes. Wingate Sandstone; Outcrop 223. On the left, equal-area projections show fault planes and slickenlines. A cross represents normal slip and an asterisk represents reverse slip. On the right, the plots show the S_1, S_2, S_3 principal stress directions, orientation of the beds and the radial (r) and tangential (t) co-ordinate directions of the dome. See text for discussion of the parameters ϕ, $\bar{\beta}$ and $\bar{\tau}$.

both normal and reverse slip directions. Indeed, when the subset of 33 normal faults is considered, $\bar{\beta}$ decreases and $\bar{\tau}$ increases, giving a good fit to a single stress tensor. The poor fit (not shown) of the subset of 13 reverse faults to a single stress tensor precludes their further analysis.

The radial distance of the outcrop from the center of the dome (1.1 km) corresponds to zone A of the elastic plate model (Fig. 11b). Within zone A at the top of a layer, plate theory predicts that σ_1 ($=\sigma_a$) will be perpendicular to the beds; it is compressive and unchanged by flexure. The in-plane principal stresses predicted by bending theory are radial and tangential. Flexure contributes a tensional change, such that both are less compressive than σ_1 and nearly equal in magnitude with $\sigma_3 = \sigma_a + \sigma_t$ and $\sigma_2 = \sigma_a + \sigma_r$. The relative magnitudes and orientations of the stresses computed from the subset of normal faults (Fig. 13) correlate well with this state of stress. The direction of S_1 is normal to the beds; S_2 lies within the plane of the beds and is approximately radial to the dome; and S_3 lies within the plane of the beds and is approximately tangential. The tangential tension, S_3, is greater than the radial tension, S_2, and their difference is very small, consistent with plate theory (Fig. 11b).

Central limb of the flexure, Mount Holmes. Within the central limb of the flexure at Mount Holmes, subradially and obliquely-striking oblique-slip faults with both normal and reverse components of slip cut by the Navajo Sandstone, which dips 20° to the WNW (outcrop 217; Figs. 2c & d and 13). Many faults have nearly horizontal slickenlines, indicating large components of strike-slip displacement. A bedding-plane fault zone directely overlies the outcrop, suggesting that outcrop 217 lies near the top of a mechanical layer. The fit of the entire population of 47 faults to a single stress tensor is good ($\bar{\beta} = 18.7°$, $\bar{\tau} = 0.84$): the stress states associated with subsets of faults with normal and reverse components of slip do not give substantially better results.

The radial distance of the outcrop from the center of the dome (2.6 km) corresponds to zone B of the elastic plate model (Fig. 11b). At this location with zone B at the top of a layer, the relative magnitudes of the in-plane stresses are small: σ_t is tensile and σ_r is slightly compressive. The state of stress computed from the faults (Fig. 13a) shows that the maximum compression, S_1, trends approximately radially and plunges to the SE. Both S_2 and S_3 are tensile and neither lies in the plane of the beds.

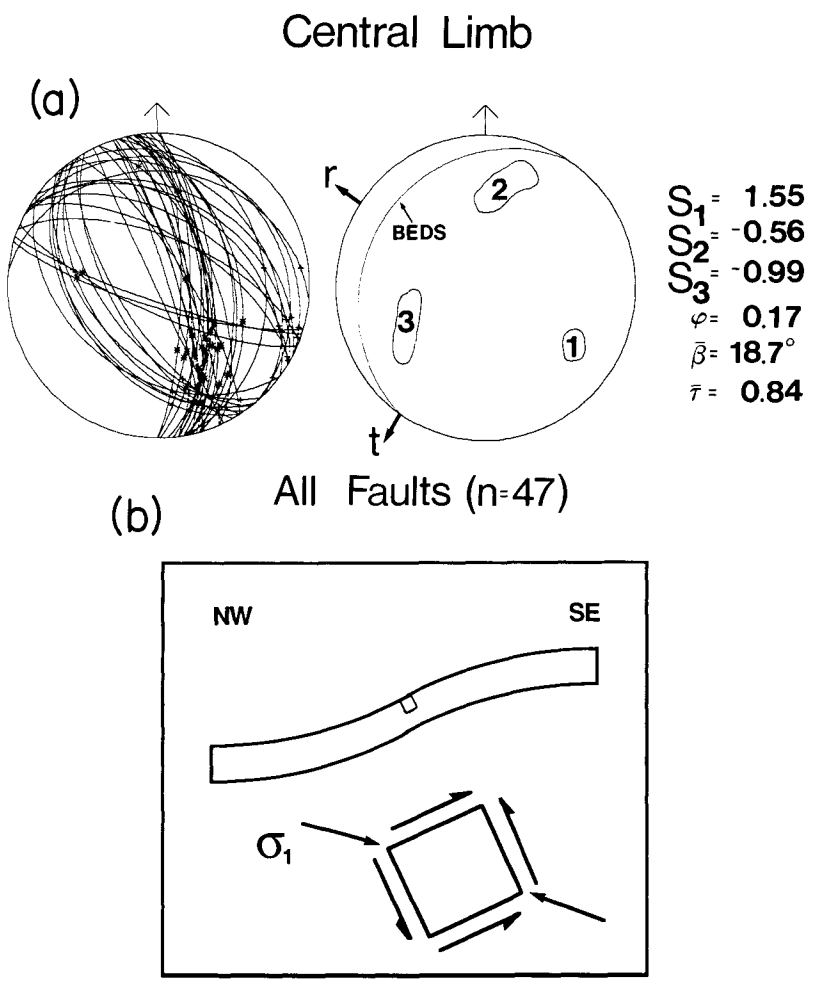

Fig. 13. (a) Fault data and computed stress axes within the central limb of the flexure at Mount Holmes. Navajo Sandstone, outcrop 217. See Fig. 12 for description of plot symbols. (b) Sketch of the configuration of stresses within an element from the central limb of a bent layer undergoing layer-parallel shear.

These computed principal stresses are not in agreement with plate-bending theory for the top of a mechanical layer in zone B. The theory predicts that σ_r should only be slightly compressive within the central limb, yet radial compression (S_1) dominates the computed state of stress. However, plate theory also predicts that the magnitudes of the bending stresses are smallest within zone B, where the curvature of the layer is small. If the mechanical layers slipped over one another during flexure, layer-parallel shear should be most important within the central limb (Fig. 13b); this shear should be associated with a maximum compression direction that plunges to the SE. The SE-plunging S_1 computed for the faults and the presence of a well-developed bedding-plane fault zone directly overlying outcrop 217, correlates well with this state of stress.

Lower hinge of the flexure, Mount Holmes. At the transition from the lower hinge to the central limb of the flexure at Mount Holmes, sub-radially and obliquely-striking normal and reverse oblique-slip faults cut the Navajo Sandstone, which dips 20° to the WNW (outcrop 220; Figs. 2a & b and 14). The three observed offsets between pairs of these faults are ambiguous as to the relative age relations of the normal and reverse slip. A thick bedding-plane fault zone occupies the upper part of the outcrop, at the contact of the Navajo Sandstone with the Carmel Formation, and several thin bedding-plane faults traverse the outcrop. A major bedding-plane fault zone also exists below this outcrop, near outcrop 217 (Fig. 2). The fit of the entire population of 40 faults to a single stress tensor is poor, $\bar{\beta} = 54.9°$, $\bar{\tau} = 0.39$ (Fig. 14). When the data are subdivided into subsets of 22 normal and 18 reverse faults, $\bar{\beta}$ decreases and $\bar{\tau}$ increases, indicating a better fit to two distinct stress tensors (Fig. 14).

The radial distance of the outcrop from the center of the dome (3.1 km) corresponds to zone B in the elastic plate model (Fig. 11b). However, the stress tensor computed from the normal faults correlates with the predicted stress state near the bottom of a layer in zone C, $\sigma_1 = \sigma_a$, $\sigma_2 = \sigma_a + \sigma_t$, and $\sigma_3 = \sigma_a + \sigma_r$. The set of faults with reverse displacements generates a state of stress compatible with that predicted by bending theory at the top of the layer within zone C. That is, $\sigma_3 = \sigma_a$ plunges steeply, $\sigma_2 = \sigma_a + \sigma_t$ and $\sigma_1 = \sigma_a + \sigma_r$, where both σ_t and σ_r are compressive. Note, however, that the poor fit of the reverse fault data to a single stress tensor ($\bar{\beta} = 30.7°$m $\bar{\tau} = 0.55$) suggests a complicted stress history within the outcrop. The analysis suggests that the

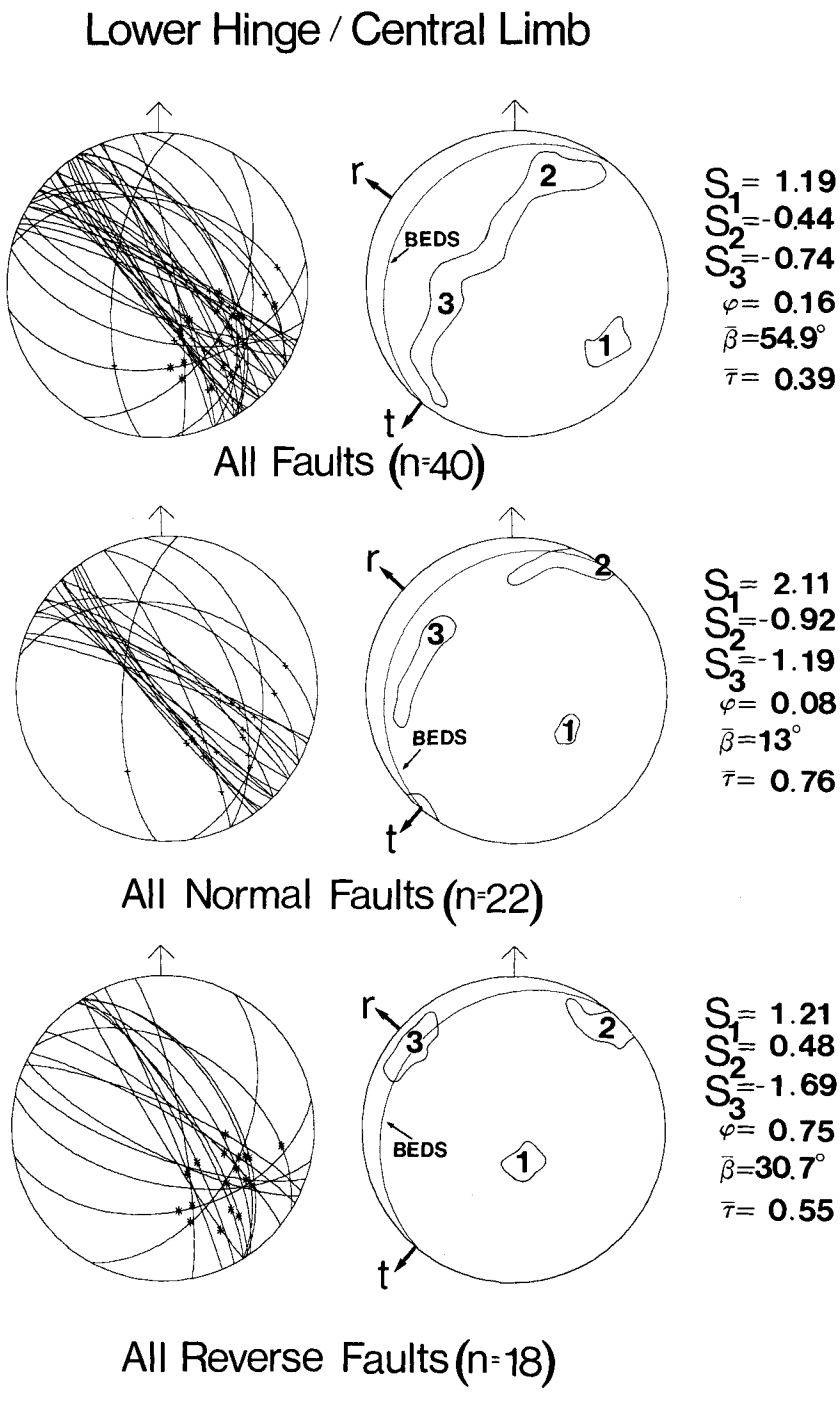

Fig. 14. Fault data and computed stress axes at the transition from the lower hinge to the central limb of the flexure at Mount Holmes. Navajo Sandstone, outcrop 220. See Fig. 12 for description of plot symbols.

rocks were deformed in at least two very different states of stress, such that σ_1 and σ_3 exchanged positions during the faulting. We hypothesize that if bedding-plane faults slipped at different horizons within the layered host rocks and the thicknesses and boundaries of mechanical layers changed repeatedly during the deformation (Price 1967), the principal stresses within the outcrop could have varied accordingly. The absence of systematic cross-cutting relations between the normal and reverse faults is consistent with the concept of alternating stress states.

Peripheral limb of the flexure, Mount Ellsworth. At the periphery of the flexure at Mount Ellsworth, about 3.2 km from the center of the dome, sandstone beds of the Entrada Sandstone dip 7° to the WNW (outcrop 233; Figs. 3a & b). These beds are cut by four sets of subradially and tangentially-striking normal faults and rare reverse faults (Fig. 15). The normal fault pattern has an orthorhombic symmetry that bears a strong resemblance to the model developed by Reches (1983) for accommodation of slip along faults in experiments with multiaxial strain fields. We observe no bedding-plane faults, so the height of the outcrop within a mechanical layer is not known. The fit of the entire population of 36 faults to a single stress tensor is poor (Fig. 15), as shown by the relatively large value of $\bar{\beta}$ (=27.7°) and the small value of $\bar{\tau}$ (=0.74). However, the subset of 31 normal faults

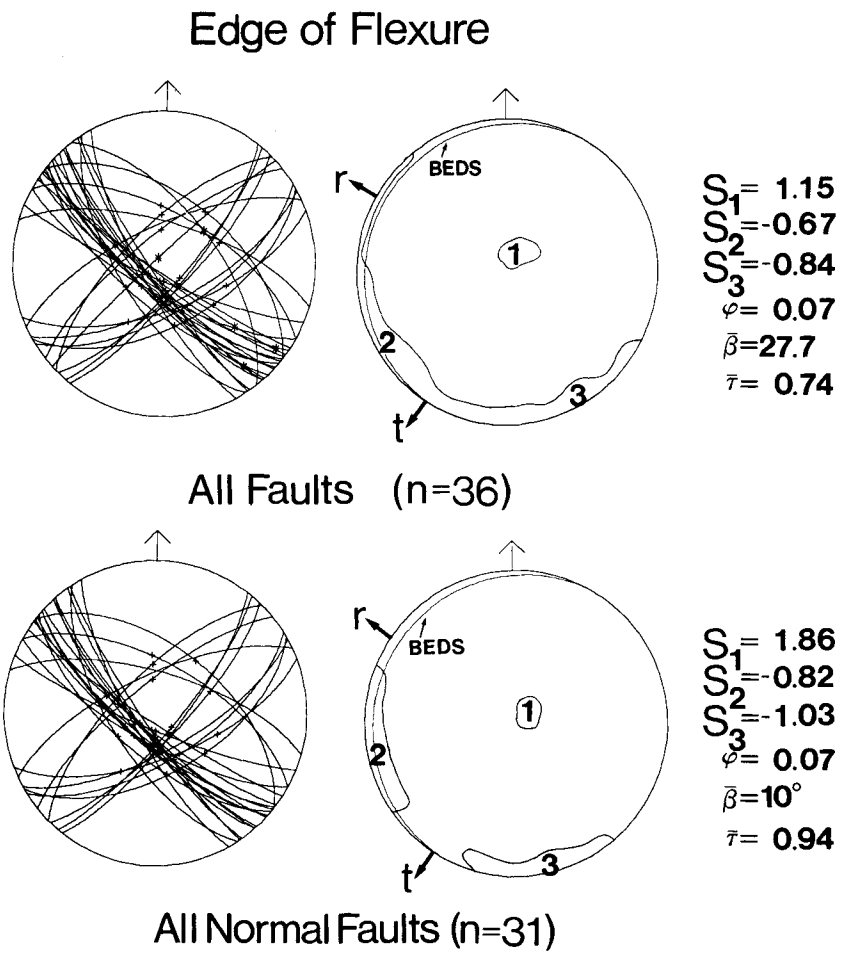

Fig. 15. Fault data and computed stress axes for all faults and normal faults, periphery of the flexure at Mount Ellsworth. Entrada Sandstone, outcrop 233. See Fig. 12 for description of plot symbols.

yields a stress tensor with S_1 vertical and the two horizontal principal stresses nearly equal in magnitude (Fig. 15), giving values of $\bar{\beta} = 10°$ and $\bar{\tau} = 0.94$. The orientations of S_2 and S_3 are not well defined because $S_2 \sim S_3$ ($\phi = 0.07$).

The radial distance of this outcrop from the center of the dome corresponds to zone C of the elastic plate model (Fig. 11b). The computed stress tensors suggest that this outcrop may lie near the bottom of a mechanical layer. There, plate theory predicts that $\sigma_1 = \sigma_a$ is compressive and unchanged by flexure. The in-plane principal stresses are tangential and radial; flexure contributes a tension, such that both are less compressive than σ_1, and the radial component, $\sigma_3 = \sigma_a + \sigma_r$, is less compressive than the tangential component, $\sigma_2 = \sigma_a + \sigma_t$. The maximum compressive stress direction predicted by plate theory, σ_1, is vertical and coaxial with S_1 computed by the faulting theory. Although S_2 and S_3 are both tensile and horizontal, their orientations do not agree with σ_2 and σ_3.

Further subdivision of these normal faults into radial and tangential sets (Fig. 16) does not significantly improve the fit of the data. It does, however, demonstrate that the radial fault set is associated with a stress state in which the least compressive principal stress, S_3, was tangential. The tangential fault set is associated with a radial S_3. The indicated difference in magnitudes of S_2 and S_3 is greater for these two subsets than for their combination. Perhaps the increase in compressive stress in the radial direction due to dip-slip displacements on certain tangential faults was sufficient for the tangential stress to become the least compressive principal stress. If so, certain radial normal faults would then slip, leading to sufficient stress change for S_3 to revert to a radial orientation. In three instances at this outcrop, tangential faults offset radial faults, and in one instance a radial fault offsets a tangential fault. These are insufficient data to be conclusive, but the ambiguous age relations are consistent with the concept of alternating states of stress.

The state(s) of stress associated with the small faults at the edge of the flexure at Mount Ellsworth is in relatively good agreement with that predicted by plate-bending theory for the bottom of a mechanical layer. Because no bedding-plane faults are exposed, however, we cannot determine the height of outcrop 233 within a mechanical layer. Jackson & Pollard (1988) estimated a radial extension of about 12% for the upper part of the cross-section at Mount Ellsworth. Circumferential and radial tension from stretching of layers over the dome will give approximately the same stress state as that predicted by bending theory for the bottom of a mechanical layer within zone C, so we cannot uniquely identify the origin of the computed state of stress. The principal stress directions lie within the plane of the beds, however, so

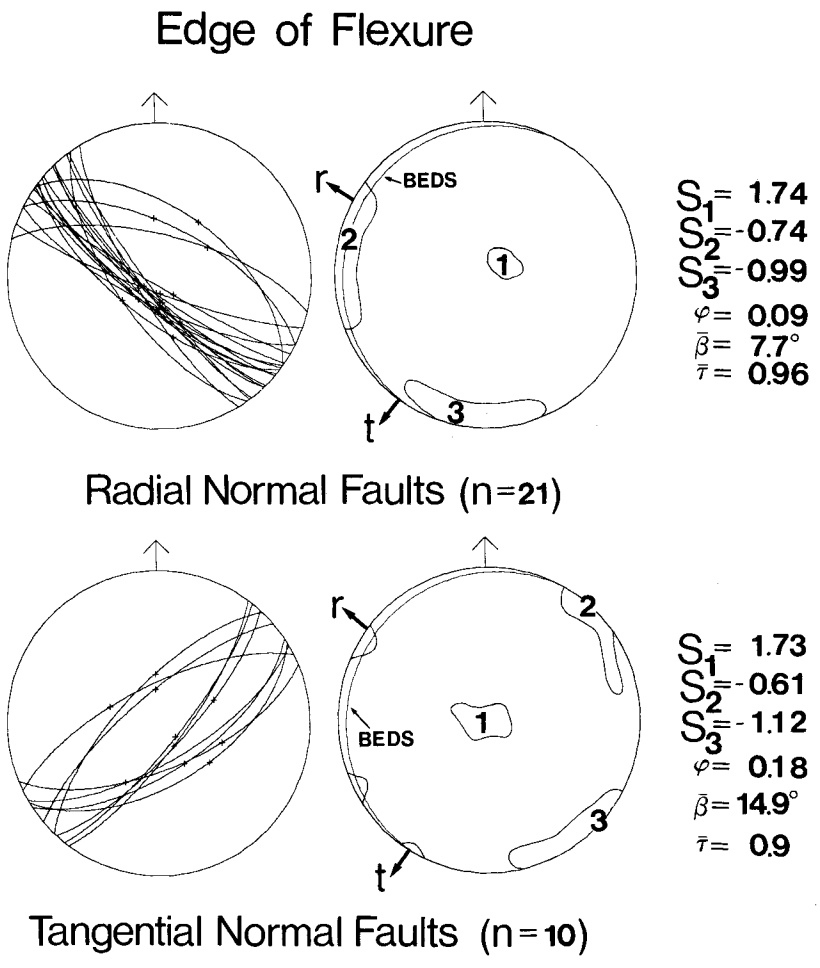

Fig. 16. Fault data and computed stress axes for radial and tangential fault sets, periphery of the flexure at Mount Ellsworth. Entrada Sandstone, outcrop 233. See Fig. 12 for description of plot symbols.

the effect of layer-parallel shear appears to have been small.

Discussion

We emphasize that the pattern of slip along the networks of outcrop-scale faults was complex. For example, only within the central limb of the flexure at Mount Holmes (outcrop 217; Fig. 13) does the fit of the entire population of faults measured within an outcrop give an acceptable fit to a single stress tensor. Within the upper hinge at Mount Holmes (outcrop 223; Fig. 12) and at the edge of the flexure at Mount Ellsworth (outcrop 233; Fig. 15), more faults have normal components of slip than reverse components and the cross-cutting relations between these faults are either ambiguous or unknown. The stress tensors computed from the normal faults alone are nearly identical with those computed for the total samples except that the error limits are smaller. From this we infer that a systematic state of stress prevailed within these outcrops but that perturbations did occur, as recorded by the faults with reverse components of slip.

At the transition from the lower hinge to the central limb of the flexure at Mount Holmes (outcrop 220; Fig. 14), there are nearly as many reverse faults as normal faults, with no consistent sense of offsetting relations. These two samples produce very different stress tensors, each of which is in agreement with bending theory, while the stress tensor associated with the total population of faults does not have a straightforward interpretation and has a larger error. From this we infer that at least two different states of stress existed within this outcrop; we suggest that there could have been a cyclical alternation of stress states as slip occurred on bedding-plane faults above and below the outcrop (Price 1967).

We have found that, in certain outcrops, stress states computed from fault data may be favorably compared with the theoretical distribution of stresses resulting from bending of a thin, circular, elastic plate with stress-free layer boundaries. In reality, the overburden behaved as a multilayer, and normal and shear stresses were transmitted across layer boundaries. The normal stress is included, as σ_a, explicitly in the bending analysis but we only qualitatively account for these shear stresses. Furthermore, a large degree of uncertainty is introduced by lack of independent evidence for vertical position within a mechanical layer. Thus, the states of stress within the mechanical layers were certainly more complex than those portrayed within the single elastic plate (Fig. 11). This and the fact that frequent perturbations in the state of stress must have occurred as

mechanical boundaries migrated, map-scale faults slipped, dikes intruded, and so on, may account for many of the less systematic aspects of the faulting data.

ADVANCED STAGES OF DOMING: MOUNT ELLSWORTH AND MOUNT HILLERS

Fault and slickenline orientation data from the host-rock flexures at Mount Ellsworth and Mount Hillers illustrate how the pattern of faulting changed with progressive inflation of the domes. The steep dips of beds within these flexures (Figs. 3 and 4) preclude comparison to a simple elastic plate model. However, the data do suggest how the faulting accommodated strains imposed by the growing intrusions.

Mount Ellsworth

About 3.2 km from the center of the dome, the Entrada Sandstone (outcrop 233, Figs. 1 and 3) dips 7°, and normal faults in four orientations offset the beds (Figs. 3a & b and 15). The four sets of faults dip steeply: the SW- and NE-dipping sets strike radially to the dome, and the NW- and SE-dipping sets strike tangentially. Slickenlines plunge steeply, giving predominantly dip-slip normal faults. The stress analysis (Figs. 15 and 16) indicates that this faulting pattern is associated with vertical compression normal to the beds and less compressive in-plane horizontal principal stresses. A few (five) dip-slip faults also cut the beds. Although this outcrop lies within the upper part of the Entrada Sandstone, we observed no bedding-plane faults.

Within the lower hinge of the flexure, the Entrada Sandstone (outcrop 202; Fig. 3) dips 30° NW and has excellent cliff and slickrock exposures of structures within individual faults. Most of these faults strike within 40° of the radial direction of the dome, and they dip to the NE and SW (Figs. 3c & d). Faults with both reverse and normal components of slip display either SE-plunging slickenlines, as observed at Mount Holmes, or they may have slickenlines that plunge to the NW, in the same direction as the dip direction of the beds (Fig. 10). Ten offsets between normal and reverse faults with SE-plunging lineations show no regular pattern. Faults with NW-plunging lineations offset faults with SE-plunging lineations in three of four cases. Occasional, thin bedding-plane faults occupy truncating surfaces between large aeolian paleodunes. A fault zone that parallels the contact with the Carmel Formation occupies the lower 5–10 m of the Entrada Sandstone, suggesting that bedding-plane slip was important at this horizon.

The Navajo Sandstone, Kayenta Formation and Wingate Sandstone (outcrops 201, 200 and 203) form the slightly curving central limb of the flexure, which dips about 48° NW with the Navajo Sandstone and 55° NW within the Kayenta and Wingate outcrops (Fig. 3). The outcrop-scale faults at all three localities strike within 60° of the radial direction of the dome and dip predominantly to the W or SW; only with the Navajo Sandstone are there a few faults that dip to the NE. At the Navajo outcrop (outcrop 201) the plunges of both the SE and NW slickenlines range from 60° to 3°, giving strike-slip and oblique-slip normal and reverse faults (Fig. 3). At the Kayenta (outcrop 200) and Wingate (outcrop 203) outcrops, the SE-directed slickenlines plunge more steeply (Figs. 3g–j). The NW-directed slickenlines plunge more gently than those at the Navajo outcrop, giving predominantly strike-slip displacements. Several bedding-plane faults traverse these outcrops, and others occupy the contacts between the formations. In seven cases, the bedding-plane faults are offset by the high-angle faults.

The Moss Back Member of the Upper Triassic Chinle Formation (outcrop 207) is the stratigraphically deepest sandstone unit in which we measured the small faults at Mount Ellsworth. The faults vary in orientation, although most have sub-radial or tangential orientations (Figs. 3k & l). Because the sandstone contains few bedding planes, and because slickenlines are not exposed, we could obtain little directional information about the slip.

Mount Hillers

At the Mount Hillers dome, measured samples of faults lie within the nearly vertical central limb of the flexure, along a traverse trending nearly N–S, roughly parallel to the host-rock cross-section (Fig. 4). The small faults strike at high angles to the beds and have the same orientations relative to the beds as those at Mount Holmes and Mount Ellsworth: faults with northwardly-plunging slickenlines measured at Mount Hillers correspond to faults with southeastwardly-plunging slickenlines measured along NW-trending traverses at the other two mountains.

The Upper Cretaceous Dakota Sandstone crops out at the periphery of the flexure, where the beds dip gently, about 9° S (outcrop 251; Fig. 4). There, the small faults strike either sub-radially and dip steeply or dip gently and have orientations similar to those of the beds (Figs. 4a & b). Slip directions, where measured, trend predominantly sub-radially.

In the Entrada Sandstone (outcrop 213), located within the central limb of the flexure, the beds dip about 87°S. Both normal and reverse faults dip steeply to the WNW and ESE and have slickenlines that trend to the NNE and plunge more steeply than the bedding normal (Figs. 3c & d). These faults offset one another with no consistent pattern. Within the steeply-dipping Navajo, Kayenta and Wingate Sandstones (outcrops 215, 211 and 214), the faults also strike sub-radially and dip steeply to the WNW or ESE (Figs. 4e, g & i). There, slickenlines trend sub-radially and plunge at almost every orientation within the radial plane (Figs. 4f, h & j). In the Navajo Sandstone, some faults with northwardly-directed slickenlines offset faults with southerly-directed slickenlines. Throughout the central limb, bedding-plane faults have mixed offsetting relations with the sub-radial faults.

Kinematics of the deformation

The bedding-plane fault zones at Mount Ellsworth occur at approximately the same stratigraphic horizons as at Mount Holmes (Figs. 2 and 3) but are more closely spaced, about 100–150 m vs 150–200 m apart at Mount Holmes. Although the thinner mechanical layers at Mount Ellsworth may have arisen from original sedimentary thickness variations, the difference may result from a greater amount of stretching during doming. Jackson & Pollard (1988) estimated a radial extension of about 12% over the upper part of the cross section at Mount Ellsworth. This implies that a complex pattern of strain resulting from both layer flexure and stretching existed within individual layers. By the time the beds dipped 50° within the central limb of the Mount Ellsworth dome, high-angle faults had begun to traverse mechanical layer boundaries and offset the bedding-plane faults. Apparently, layer-parallel slip had diminished significantly relative to slip on the high-angle fault networks by the final stages of uplift at Mount Ellsworth.

On the south flank of Mount Hillers, numerous steeply-dipping bedding-plane faults crop out within the near-vertical central limb of the dome. The spacing of these faults is not well-known, however. Their mixed offsetting relations with faults that cut the bedding at high angles suggest that renewed slip occurred along some of the bedding-plane faults as the central limb of the flexure steepened to its present orientation.

Faulting at the outcrop scale during the later stages of doming at Mount Ellsworth and Mount Hillers was dominated by high-angle faults with normal and reverse components of slip. As at Mount Holmes, most of these faults have slickenlines that plunge in the same general direction as the bedding normal. These faults form subset A of the population (Fig. 10a). Other faults have slickenlines that plunge in the same general orientation as the dip directions of the beds. Faults with this sense of slip form subset B of the population (Fig. 10b); these occur only in the more advanced stages of flexure.

At least some of the subset B faults must have slipped in their present orientations, because their slickenlines plunge more steeply than is possible by rotation from subset A orientations. Displacements along these faults probably accommodated outward pushing of the host rock as the intrusions inflated. On the other hand, the large range of slickenline orientations within the nearly vertical beds at Mount Hillers suggests that some of the subset B faults slipped in the subset A direction and were then rotated to their present orientations as the beds steepened. Even so, some subset A faults offset subset B faults, indicating that faulting with displacements directed towards the bed normal continued throughout the doming.

DISCUSSION AND CONCLUSIONS

In the early stage of intrusion, well before vertical displacements reached those observed at Mount Holmes (Fig. 2), we hypothesize that the sedimentary overburden behaved as a massive elastic body that deformed in response to pressure from a thin, underlying sill (see Jackson & Pollard 1988, fig. 19A). As increasingly high shear stresses relative to normal stresses developed on weak bedding planes over the periphery of the sill, bedding-plane faults nucleated and began to slip. These faults subdivided the overburden into thin mechanical layers that were more easily flexed as the transition to a laccolithic form of intrusion began. By the final stage of deformation at Mount Holmes, the overburden was subdivided into mechanical layers about 200 m thick, so that thickness-to-length ratios were very small. Flexure of sedimentary host rocks at the three southern Henry Mountains domes was accommodated, in part, by slip along bedding-plane faults and a network of closely-spaced, steeply-dipping normal and reverse oblique-slip faults. Stress analysis of fault-population data suggest that displacements along the networks of high-angle outcrop-scale faults accommodated bending stresses within these mechanical layers. Earlier workers (Pollard & Johnson 1973, Dixon & Simpson 1987, Koch *et al.* 1981) concluded that flexure of overburden layers was important in determining the shape of monoclines over small laccoliths. Our analysis suggests that this is the case for the early stages of growth of larger laccoliths, as well.

With progressive growth of the domes from the stage of multilayer flexure observed at Mount Holmes (Jackson & Pollard 1988, fig. 19B), the bedding-plane faults continued to slip. However, by the final stage of deformation at Mount Ellsworth, where beds within the central limb of the flexure dip 50–55°, high-angle faults offset most bedding-plane faults, and slippage along mechanical layers appears to have diminished. At this stage of large-amplitude doming, the layers had been stretched, as well as bent into their final configurations. Some high-angle faults continued to slip in the same orientations as those at Mount Holmes, in the direction of the bed normal, suggesting that bending and flexure were important over the full range of deformation. In addition, strike-slip and oblique-slip displacements directed toward the bed dip direction along similarly oriented faults accommodated strains resulting from outward inflation of the growing magma chamber.

Older faults and their slickenlines were rotated as the beds steepened. Rotation of the central limb at Mount Hillers about a horizontal axis at the lower hinge became an important component of the deformation. There, displacements along the fault networks are not substantially larger than those at Mount Ellsworth, despite the increased vertical deflection of the strata. At all three domes the fault networks are best exposed within the central limbs of the flexures. It is difficult to estimate whether the intensity of faulting is greatest within the hinges of the flexures because, in general, these areas are not well exposed. Positions of the hinges in the cross-sections of Mount Holmes, Mount Ellsworth and Mount Hillers remain nearly constant, suggesting that little migration of the hinges occurred during the later stages

of doming. The abundant, steeply-dipping, map-scale faults exposed over the top of Mount Ellsworth are indicative of late-stage jostling of fault blocks over the central magma chamber. Many radial dikes 5–15 m thick cut the central parts of the domes; these accommodated some of the circumferential stretching of the sedimentary host rocks.

Acknowledgements—This paper benefited from reviews by D. De Paor, Z. Reches, J. Dixon, D. Hyndman, E. Anderson and A. Michael. P. Delaney assisted with computerized plots of stereographic projections of fault data. This research formed part of Jackson's Ph.D. dissertation, and was funded, in part, by the Department of Earth and Planetary Sciences at Johns Hopkins University.

REFERENCES

Anderson, E. M. 1951. *The Dynamics of Faulting and Dyke Formation with Applications to Britain* (2nd edn). Oliver and Boyd, Edinburgh.

Angelier, J. 1979. Determination of the mean principal directions of stresses for a given fault population. *Tectonophysics* **56**, 17–26.

Armstrong, R. L. 1969. K–Ar dating of laccolithic centers of the Colorado Plateau and vicinity. *Bull. geol. Soc. Am.* **80**, 2081–2086.

Aydin, A. 1978. Small faults formed as deformation bands in sandstone. *Pure & Appl. Geophys.* **116**, 913–930.

Aydin, A. & Johnson, A. M. 1978. Development of faults as zones of deformation bands and slip surfaces in sandstone. *Pure & Appl. Geophys.* **116**, 931–942.

Byerlee, J. D. 1978. Friction in rocks. *Pure & Appl. Geophys.* **116**, 615–626.

Clark, S. P., Jr. 1966. Handbook of physical constants. *Mem. geol. Soc. Am.* **97**.

Dixon, J. M. & Simpson, D. G. 1987. Centrifuge modelling of laccolithic intrusion. *J. Struct. Geol.* **9**, 87–103.

Erickson, L. L. 1987. A three-dimensional dislocation program with applications to faulting in the earth. Unpublished M.S. thesis, Stanford University.

Gilbert, G. K. 1877. Report on the Geology of the Henry Mountains. *U.S. Geog. & Geol. Surv. Rocky Mountain Region.*

Hunt, C. B. 1953. Geology and geography of the Henry Mountains region, Utah. *Prof. Pap. U. S. geol. Surv.* **228**.

Hyndman, D. W. & Alt, D. 1987. Radial dikes, laccoliths and gelatin models. *J. Geol.* **95**, 763–774.

Jackson, M. D. 1987. Deformation of host rocks during growth of igneous domes, southern Henry Mountains, Utah. Unpublished Ph.D. dissertation, Johns Hopkins University.

Jackson, M. D. & Pollard, D. D. 1988. The laccolith–stock controversy: new results from the southern Henry Mountains, Utah. *Bull. geol. Soc. Am.* **100**, 117–139.

Koch, F. G., Johnson, A. M. & Pollard, D. D. 1981. Monoclinal bending of strata over laccolithic intrusions. *Tectonophysics* **74**, 21–31.

Michael, A. 1984. Determination of stress from slip data: faults and folds. *J. geophys. Res.* **89**, 11517–11526.

Oppenheimer, D. H., Reasenberg, P. A., Simpson, R. W. 1988. Fault plane solutions for the 1984 Morgan Hill, California, earthquake sequence: evidence for the state of stress on the Calaveras fault. *J. geophys. Res.* **93**, 9007–9026.

Pollard, D. D. & Johnson, A. M. 1973. Mechanics of growth of some laccolithic intrusions in the Henry Mountains, Utah, II: bending and failure of overburden layers and sill formation. *Tectonophysics* **18**, 261–309.

Price, R. A. 1967. The tectonic significance of mesoscopic subfabrics in the southern Rocky Mountains of Alberta and British Columbia. *Can. J. Earth Sci.* **4**, 39–70.

Ramsay, J. G. 1967. *Folding and Fracturing of Rocks*. McGraw-Hill, New York.

Reches, Z. 1983. Faulting of rocks in three dimensional strain fields II. Theoretical Analysis. *Tectonophysics* **95**, 133–156.

Reches, Z. 1987. Determination of the tectonic stress tensor from slip along faults that obey the Coulomb yield criterion. *Tectonics* **6**, 849–861.

Segall, P. & Pollard, D. D. 1980. Mechanics of discontinuous faults. *J. geophys. Res.* **85**, 4337–4350.

Segall, P. & Pollard, D. D. 1983. Nucleation and growth of strike-slip faults in granite. *J. geophys. Res.* **88**, 555–568.

Sullivan, K. R. 1987. Igneous intrusions in southeastern Utah: relation to space–time–composition patterns of Cenozoic igneous activity in Nevada, Utah and Colorado. *Geol. Soc. Am. Abs. w. Prog.* **19**, 337.

Timoshenko, S. & Woinowsky-Krieger, S. 1953. *Theory of Plates and Shells*. McGraw-Hill, New York.

Withjack, W. O. & Scheiner, C. 1987. Fault patterns associated with domes–an experimental and analytical study. *Bull. Am. Ass. Petrol Geol.* **66**, 302–316.